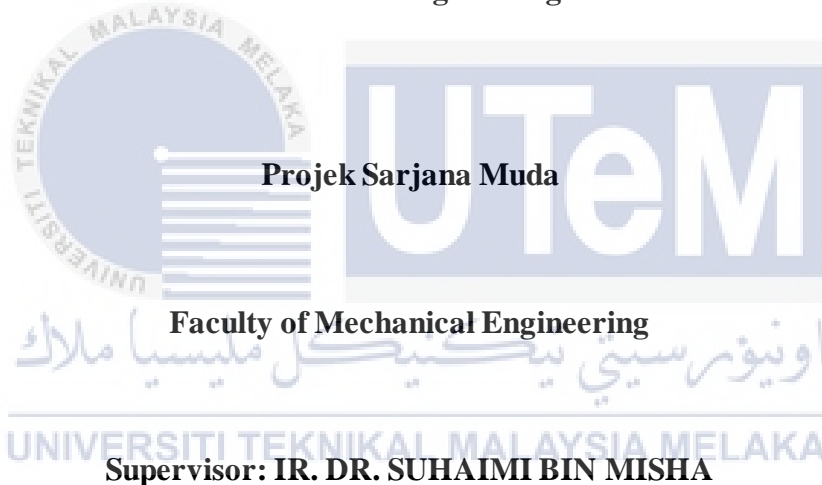


**STUDY THE EFFECT OF FIN ON SOLAR COLLECTOR PERFORMANCE USING
CFD SIMULATION**

EFFY RUSHDANE AFFANDI BIN HASNALEE

**A report submitted
In fulfillment of the requirement for the degree of
Bachelor of Mechanical Engineering with Honours**



UNIVERSITI TEKNIKAL MALAYSIA MELAKA

JANUARY 2022

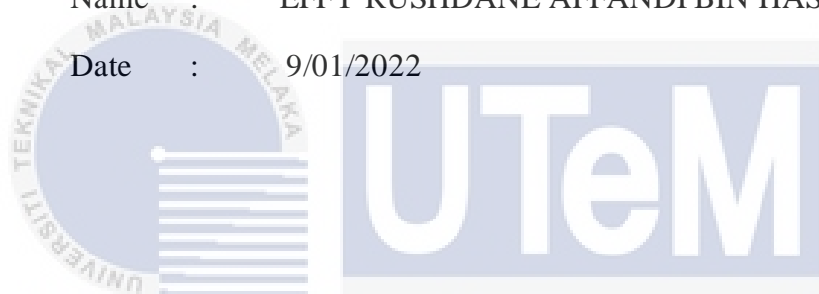
DECLARATION

I declare that this project report, "Study the Effect of Fin on Solar Collector Performance Using CFD Simulation," is entirely my work, except for the references.

Signature: 

Name : EFFY RUSHDANE AFFANDI BIN HASNALEE

Date : 9/01/2022



اونيورسيتي تيكنيكل مليسيا ملاك

UNIVERSITI TEKNIKAL MALAYSIA MELAKA

APPROVAL

I hereby certify that I have reviewed this project report and believe it to be adequate in scope and quality for the award of the Bachelor of Mechanical Engineering degree.

Signature :

Name of Supervisor :

Date :



اونيورسيتي تيكنيكل مليسيا ملاك

UNIVERSITI TEKNIKAL MALAYSIA MELAKA

DEDICATION

To my beloved parents, family and myself.



ABSTRAK

Secara amnya, pengumpul udara solar digunakan untuk menangkap tenaga haba untuk pengeringan. lazimnya, pengumpul udara solar tradisional termasuk penyerap untuk menangkap haba daripada sinaran matahari. Walau bagaimanapun, dalam keadaan tertentu, haba yang dikumpul oleh pengumpul udara solar tradisional adalah tidak mencukupi kerana beberapa faktor seperti iklim dan tujuan haba dikumpul. Prestasi pengumpul udara solar boleh dipertingkatkan dengan mengubah komponen yang digunakan untuk menyerap haba dengan menambah sirip pada penyerap pengumpul. Tujuan penyelidikan ini adalah untuk menentukan pengaruh sirip pada pengumpul suria. Objektif utama kerja ini adalah untuk membangunkan, memeriksa, dan menganalisis prestasi terma segi empat tepat, beralun, alur-v dan mendatar susunan sirip pengumpul suria menggunakan pengiraan dinamik bendalir secara komputasional (CFD). Tujuan simulasi CFD adalah untuk menentukan pengaruh sirip pada kenaikan suhu, tekanan, dan halaju aliran bendalir dalam pengumpul suria dengan mensimulasikan keadaan fizikal sesuatu kajian model pengumpul udara solar. Dapatan kajian menunjukkan bahawa sirip segi empat tepat, sirip beralun, sirip alur berbentuk v, dan sirip mendatar semuanya mempunyai kenaikan suhu yang lebih tinggi daripada model kajian, pada 5.4 peratus, 5.6 peratus, dan 5.3 peratus, masing-masing, manakala sirip mendatar mempunyai yang paling tinggi kenaikan suhu pada 5.7 peratus, berbanding model kajian 4.2 peratus. Kesimpulannya, kajian ini menyimpulkan bahawa sirip mendatar memberikan peningkatan haba yang terbaik, tetapi segi empat tepat sirip adalah pilihan yang lebih baik dalam keadaan dan aplikasi yang setanding dengan model kajian.

اونيورسيتي تيكنيكل مليسيا ملاك

UNIVERSITI TEKNIKAL MALAYSIA MELAKA

ABSTRACT

Typically, a solar air collector is used to capture thermal energy for drying. Typically, a traditional solar air collector includes an absorber to capture heat from the sun's rays. However, under certain circumstances, the heat gathered by a traditional solar air collector is insufficient due to considerations such as climate and the purpose of the collector. A solar collector's thermal performance can be enhanced by altering the material used to absorb heat, for as by adding fins to the collector's absorber. The purpose of this research is to determine the influence of fins on a solar collector. The primary objective of this work is to develop, examine, and analyze the thermal performance of rectangular, wavy, v-groove, and horizontal fins arrangement solar collectors using computational fluid dynamics (CFD). The purpose of the CFD simulation is to determine the influence of fins on temperature rise, pressure, and fluid flow velocity in the solar collector by simulating the boundary conditions of a study model solar air collector. The study's findings indicate that rectangular fins, wavy fins, v-groove fins, and horizontal fins all have a higher temperature rise than the study model, at 5.4 percent, 5.6 percent, and 5.3 percent, respectively, while horizontal fins have the highest temperature rise at 5.7 percent, compared to the study model's 4.2 percent. In conclusion, the study concluded that horizontal fins provide the best thermal improvement, but rectangular fins are a better choice in a comparable circumstance and application to the study model.



ACKNOWLEDGEMENT

To begin, I would want to express my gratitude to everyone who provided me with the opportunity and helped me finish my assignment successfully. My heartfelt appreciation goes to Ir. Dr. Suhaimi bin Misha, my final year project supervisor, for his supervision, tolerance, inspiration, and support. His leadership and helpful suggestions throughout this endeavor have aided in my completion.

Second, I'd want to convey my heartfelt appreciation to my classmates, particularly Mr. Ahmad Syahir bin Ibrahim, who aided me greatly with my simulation project, and to my pals, for all the fun we had during the four years of my degree life.

Finally, I'd like to express my gratitude to my family. I would not be where I am now without their undying love and support. We appreciate your sacrifices and encouragement during my schooling.

TABLE OF CONTENTS

DECLARATION	i
APPROVAL.....	ii
DEDICATION.....	iii
ABSTRAK.....	iv
ABSTRACT	v
ACKNOWLEDGEMENT.....	vi
TABLE OF CONTENTS	vii
LIST OF FIGURES.....	x
LIST OF TABLES	xii
LIST OF EQUATIONS.....	xiii
LIST OF ABBREVIATION.....	xiv
Chapter 1	1
INTRODUCTION.....	1
1.1 Background.....	1
1.2 Problem Statement.....	3
1.3 Objective.....	3
1.4 Scope of Project.....	4
Chapter 2.....	5
LITERATURE REVIEW	5
2.1 Introduction	5
2.2 Overview of Solar Collector System and fins.....	5
2.3.1 Fins Arrangement in Double Pass Solar Collector.	10
2.3.2 Fin and Baffle Configuration	13
2.3.3 V-Groove Solar Air Collector	15
2.3.4 Flat Plate Solar Collector Performance Assessment with Internal Fins and Porous Media.....	17
2.3.5 Effect of fin pattern on the air-side performance of herringbone wavy fin-and-tube heat exchangers.....	22

2.3.6 Operative Parameters and Thermal Efficiency of Solar Collector Effect Of Fins Attachment.....	23
2.4 The Effect Of Fins.....	24
Chapter 3.....	29
METHODOLOGY.....	29
3.1 Introduction.....	29
3.2 Overview.....	29
3.3 Methodology Chart.....	30
3.4 Simulation Procedures.....	31
3.4.1 Simulation Setup.....	31
3.4.2 Boundary Conditions for The Optimization Study:.....	34
3.4.3 Numerical Method.....	34
3.4.4 Meshing.....	35
3.5 Governing Equation.....	35
3.5.1 Fluid Flow.....	36
3.5.2 Heat Transfer.....	37
Chapter 4.....	40
RESULTS AND ANALYSIS.....	40
4.1 Study Model Results.....	40
4.1.1 Results of Double Phase Solar Collector with Fins.....	40
4.1.2 Flow Trajectories of Double Phase Solar Collector with Fins.....	41
4.2 Result Validation.....	42
4.2.1 Study Model.....	42
4.2.2 CAD Model Based on Study Model.....	44
4.3 Comparison between data taken from Study Model and CFD analysis.....	46
4.4 Fin Designs and the CFD Analysis.....	48
4.4.1 Plain Fin Design (Study Model).....	50
4.4.2 Rectangular Fins.....	52

4.4.3 Wavy Fins	54
4.4.4 V- Groove Fins.....	57
4.4.5 Horizontal Fins.....	60
4.5 Results Discussion	62
4.5.1 The Effect of Fins on Temperature Rise.....	62
4.5.2 The Effect of Fins on Pressure in Solar Collectors.....	64
Chapter 5	67
CONCLUSION.....	67
References	69



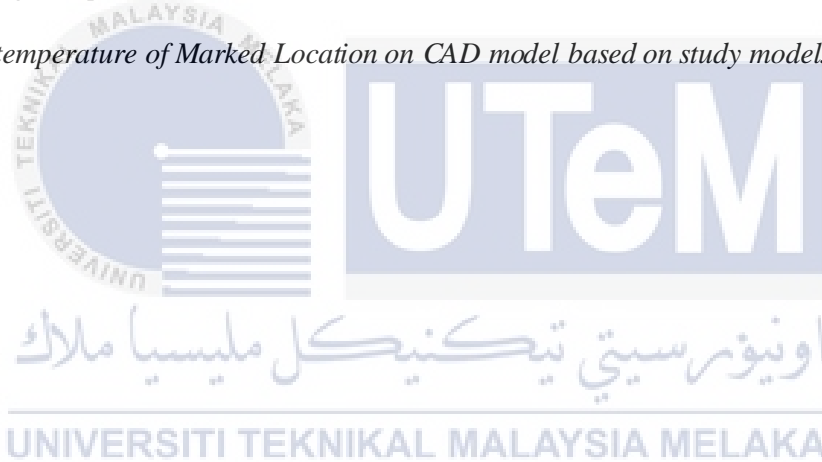
LIST OF FIGURES

<i>Figure. 2.1. Various Types of Flat-Plate Solar Collectors: A-D: Water-Based Solar Collectors, (Fudholi & Sopian, Review on Solar Collector for Agricultural Produce, 2018).</i>	6
<i>Figure. 2.2. Schematic Diagram of Experimental Setup. (Singh S., 2020).</i>	10
<i>Figure. 2.3. Details of fins arrangements (a) inline, (b) staggered, and (c) hybrid staggered. (Singh, 2020).</i>	11
<i>Figure. 2.4. 3D Models of Solar Collectors. (AFSHARI, et al., 2019).</i>	14
<i>Figure. 2.5. Meshed view of solar collectors. (AFSHARI, et al., 2019).</i>	15
<i>Figure. 2.6. Cross-Sectional View of v-groove. (Karim & Hawlader, 2005).</i>	16
<i>Figure. 2.7. Schematic Diagram of flat plate collectors. (Kansara, Pathak, & Patel, 2021).</i>	18
<i>Figure. 2.8. Diagrammatic representation of (a) a solar simulator and (b) the dimensions of an infrared lamp and array layout. (Kansara, Pathak, & Patel, 2021).</i>	20
<i>Figure. 2.9. Experimental setups (a) layout (b) under operating conditions. (Kansara, Pathak, & Patel, 2021).</i>	21
<i>Figure. 2.10. The corrugated flow channel inside the heat exchanger with the wavy fin design type I and type II is depicted schematically. (Chokeman & Wongwises, 2005).</i>	22
<i>Figure. 2.11. (a) Main parts of collector type C1, (b) fins configuration on the backboard, (c) front view of the suitable overlap for the two fin groups (A: first row fins, B: second-row fins). 1: The space between the glass cover and absorber plate, 2: air passage, 3: stone wool insulator. (Daliran & Ajabshirchi, 2018).</i>	23
<i>Figure. 2.12. Variation of Collector Outlet Temperature Via Inlet Air Velocity. (AFSHARI, et al., 2019).</i>	25
<i>Figure. 2.13. Variation of temperature rise and heat absorbed by air with mass flow rate and heat flux input ((a), (b), and (c) are for case-2; (d), (e), and (f) comparison between case-1(no fins) and case-2 (with fins). (Kansara, Pathak, & Patel, 2021).</i>	26
<i>Figure. 2.14. Coefficient of heat transmission and pressure decrease. (Chokeman & Wongwises, 2005).</i>	27
<i>Figure. 3.1. Methodology Flow Chart</i>	30
<i>Figure. 3.2. Zone for optimum angles. (Khatib, Mohamed, Mahmoud, & Sopian, 2015).</i>	32
<i>Figure. 3.3. The schematic of a double-pass solar collector with fins absorber in the second channel.</i>	32
<i>Figure. 3.4. Three-dimensional model of a double-pass solar collector with fins</i>	33

<i>Figure. 3.5. Study Model in a solar drying system.</i>	33
<i>Figure. 3.6. Mesh.</i>	35
<i>Figure. 4.1. Solar Collector Study Model.</i>	40
<i>Figure. 4.2. Flow trajectories (a) top (b) bottom.</i>	41
<i>Figure. 4.3. Marked Location for Recording Data.</i>	42
<i>Figure. 4.4. Marked Location on CAD model based on study model.</i>	44
<i>Figure. 4.5. Outlet Temperatures contour on CAD model based on study model. (a) Bottom (b) Side.</i>	45
<i>Figure. 4.6. The temperature rises between the study model and CFD based on the study model.</i>	47
<i>Figure. 4.7. Fins Design (a) Rectangular (b) Wavy (c) V-groove (d) Horizontal</i>	49
<i>Figure. 4.8. (a) Temperature contour in fins region (b) Position where the results will be analyzed.</i> .50	
<i>Figure. 4.9. Study Model (a) Temperature rise (b) Velocity.</i>	51
<i>Figure. 4.10. Rectangular Fins Design.</i>	52
<i>Figure. 4.11. Temperature contour in rectangular fins region.</i>	52
<i>Figure. 4.12. Rectangular Fins (a) Temperature Rise (b) Velocity.</i>	54
<i>Figure. 4.13. Wavy Fins Design.</i>	54
<i>Figure. 4.14. Temperature Contour in Wavy Fins Region.</i>	55
<i>Figure. 4.15. Wavy Fins (a) Temperature rise (b) Velocity.</i>	56
<i>Figure. 4.16. V-groove Design.</i>	57
<i>Figure. 4.17. Temperature contour in V-groove fins region.</i>	57
<i>Figure. 4.18. V-groove Fins (a) Temperature Rise (b) Velocity.</i>	59
<i>Figure. 4.19. Horizontal Fins Design.</i>	60
<i>Figure. 4.20. Temperature Contour In horizontal fins region.</i>	60
<i>Figure. 4.21. Horizontal Fins (a) Temperature rise (b) Velocity.</i>	61
<i>Figure. 4.22. Temperature Rise comparison between different types of fins configuration.</i>	63
<i>Figure. 4.23. Pressure on different fins design configurations.</i>	66

LIST OF TABLES

<i>Table. 2.1. Design and operation parameters used in experimental work. (Singh S., 2020).</i>	12
<i>Table. 2.2. Mesh information of the computational model. (Kansara, Pathak, & Patel, 2021).</i>	19
<i>Table. 2.3. Specification of IR lamp. (Kansara, Pathak, & Patel, 2021).</i>	20
<i>Table. 2.4. The number of fins and corresponding thermal resistance to the air. (Kansara, Pathak, & Patel, 2021).</i>	27
<i>Table. 4.1. Parameters of Study Model.</i>	42
<i>Table. 4.2. Temperatures Recorded in Marked Locations.</i>	43
<i>Table. 4.3. Average temperatures at the outlet.</i>	43
<i>Table. 4.4. The temperature of Marked Location on CAD model based on study model.</i>	44



LIST OF EQUATIONS

<i>Equation 1 Continuity Equation:</i>	36
<i>Equation 2 Momentum Equation:</i>	36
<i>Equation 3 Energy Equation:</i>	36
<i>Equation 4 Required space between fins:</i>	37
<i>Equation 5 Velocity between fins:</i>	37
<i>Equation 6 Reynold number for air between fins:</i>	38
<i>Equation 7 Nusselt Number:</i>	38
<i>Equation 8 Definition of f:</i>	38
<i>Equation 9 Heat Transfer coefficient:</i>	38
<i>Equation 10 Heat Flux:</i>	39



LIST OF ABBREVIATION

CFD	Computational Fluid Dynamics
CAD	Computational Aided Design
b	Space between fins (mm)
V	Velocity of air between fins (m/s)
f_1	Friction factor
H_f	Fin height
k	Turbulent kinetic energy
K_f	Thermal conductivity of the fluid (W/mK)
L	Length of the fin (mm)
\dot{m}	Mass flow rate (kg/s)
Nu	Nusselt number
P	Pressure (Pa)
Q	Heat flux (W/m ²)
μ	Dynamic viscosity (N s/m ²)
ρ	Density (kg/m ³)
ε	Rate of dissipation of turbulent kinetic energy
Re	Reynold Number
T_i	Inlet temperature of air (K)
T_o	Outlet temperature of air (K)



Chapter 1

INTRODUCTION

1.1 Background

The world's energy demand is increasing drastically as the growth of the Earth's population soars each year. As a result, the energy demand is also growing which also sparks economic development to increase significantly. As economic development takes place, the energy demand also increases following the economic growth trend. Using non-renewable energy will not meet the energy demand since it is limited. Moreover, the use of non-renewable energy sources leads to climate change which causes natural disasters that may be harmful to the ecosystem. Therefore, renewable or eco-friendly energy sources are the way to go for the greater good of the future. Solar energy could be the best choice as energy is the most abundant renewable energy source. (Kannan & Vakeesan, 2016).

Solar energy is openly has a lot of advantages relative to any other energy source. It does not use natural resources, no carbon dioxide or other gaseous emissions into the air, or produces wastes. The advantages of solar energy are the following:

- No greenhouse gases emissions
- Recover degraded land
- Improve the quality of water resources
- Increase energy independence

(Solangi et al., 2011).

Global warming, caused by CO₂ emissions, has become a serious issue that must be monitored as global energy consumption continues to expand. Solar energy, in particular, is widely regarded as a critical component of attaining sustainable human expansion and as one of the most effective cures for global warming. Solar collectors are a type of solar energy harvesting device. The solar collector is a one-of-a-kind energy exchanger that converts solar energy directly into thermal energy from the working fluid in photovoltaic applications or into electricity in solar thermal applications. Solar radiation is captured by a solar collector and converted to heat for solar thermal applications before being transferred to the collector's working fluid (air, water, or oil). The heat transferred by the working fluid can be utilised for domestic hot water/heating or can be used to charge a thermal power storage tank from which heat can be extracted later (at night or cloudy days). Numerous non-concentrated solar collectors, such as flat solar collectors, are available. A different sort of solar collector is the concentrating collector. (Tian & Zhao, 2013).

1.2 Problem Statement

A solar energy system should be designed in such a way that it produces the appropriate amount of energy at the lowest possible cost. A flat plate collector is one of the solar energies. A flat plate heat exchanger air collector is a form of heat exchanger that receives solar radiation and converts it to heat energy. Thermal efficiency is used in this method to compare the thermal performance of solar collectors. Thermal efficiency is widely thought to be the most critical criterion for thermal performance estimation. The typical solar air collector, on the other hand, is well-known for its poor thermal performance. The study refers to a model for conducting research. Under the absorber, this model employs a simple fin structure. To improve the thermal performance of the system, it is necessary to study, build, and assess an appropriate design strategy utilizing computational fluid dynamics (CFD).

1.3 Objective

This project aims to study the effect of fins on solar collectors. This report should accomplish the following objectives:

1. To study the effect of fins on solar collectors.
2. To design, study and analyse with CFD the rectangular, wavy, v-groove and horizontal fins configuration design of solar collectors in thermal performance.
3. To compare the effect of fins on temperature rise, pressure, and the velocity of air in the solar collector.
4. To choose the appropriate fin configuration design that are suitable to improve the current study model design.

1.4 Scope of Project

The scopes of this project are:

1. Only results of solar collector that is influenced by the existence of fins are presented in this report.
2. The CFD simulation of the effect of fins on the solar collector is analysed and validated by experimental results.
3. Apart from the plain fin from the study model, the rectangular, wavy, v-groove and horizontal fins will be newly designed.



Chapter 2

LITERATURE REVIEW

2.1 Introduction

The literature review that will be used in this project will be covered in this chapter. The material will include information about solar collector systems with and without fins, fin comparisons between prior research investigations, and actual fin designs and simulation efforts.

2.2 Overview of Solar Collector System and fins

The solar collector is a critical component of a solar energy system. It is a device that collects solar energy, converts it to thermal energy, and then transfers the thermal energy to the fluid running through the collector. A flat-plate collector is a type of solar collector that is well-known. The simplest solar collector, with no glass and an uninsulated absorber plate. This collector is ideal for swimming pool heating applications where the water temperature needs to be raised merely a few degrees above the ambient air temperature (0–10 °C). As a result, heat losses are negligible. A glass or plastic cover may be used to reduce heat loss. A solar collector with glazing is composed of a cover, an absorber plate, and insulation on the bottom and sides. The cover may be used to prevent heat loss from the collector's top, and the absorber plate may be insulated to prevent heat loss from the collector's surroundings. A basic solar collector consists of a flat plate collector covered in glass and equipped with an air channel (single pass). Frequently, a black-painted absorber plate is used. In higher-temperature collectors, one or more glazing layers are commonly utilised. (Fudholi & Sopian, Review on Solar Collector for Agricultural Produce, 2018). A solar air heater is a device

designed to meet present and future mild temperature requirements for space heating, agricultural product drying, and industrial processes. (Close, 1963). Solar collectors are frequently classified into two categories based on their concentration ratios: non-concentrating and concentrating collectors. (Tian & Zhao, 2013).

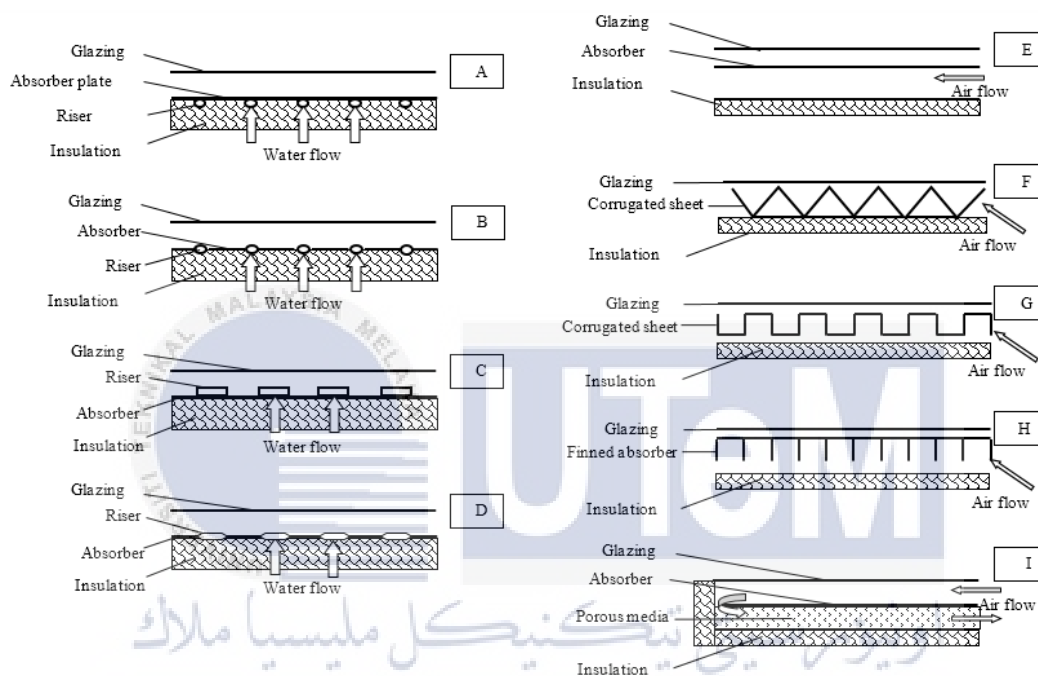


Figure 2.1. Various Types of Flat-Plate Solar Collectors: A-D: Water-Based Solar Collectors, (Fudholi & Sopian, Review on Solar Collector for Agricultural Produce, 2018).

Figure 2.1. (E) depicts a standard flat-plate collector with a clear cover, absorber, insulation, and frame. As a result, a flat-plate collector is made up of one or more glass sheets or a transparent material placed atop an absorbent plate with air flowing around it. Traditional flat-plate collectors have low thermal efficiency. To achieve a significant collector efficiency increase, enlarged heat transfer regions, such as corrugated surfaces (Figure 2.1. (F) and 2.1

(G)), finned absorbers (Figure. 2.1 (H)), and porous media (Figure 2.1. (I)), are required. (Fudholi & Sopian, 2018).

Due to ongoing research in the field of solar air heaters, a variety of designs are now available. Researchers are primarily interested in accounting for thermal losses to the environment as well as the pumping power required to maintain the airflow rate in solar air heaters. The glass covers, as well as the absorber and back plates, are the key components of traditional solar air heaters. Traditional solar air heaters that use such components, however, have poor thermal performance. (Biondi, Cicala, & Farina, 1988). As a result, increasing the air circulation duration by Mohamad (1997), and increasing the heat transfer area by attaching surfaces to the absorber plate by Momin, Saini, & Solanki (2002), are two key options documented in the literature for improving the thermal performance of traditional solar air heater designs. However, for greater thermal performance, a double glass cover is also advised. (Ho, Lin, Chuang, & Chao, 2013).

The tunnel's working fluid is circulated and heated by the hot absorber plate. Controlling the enclosure material's heat transfer resistance to any particular working fluid flowing through the route is how heat transfer is regulated. Increasing the surface area of the enclosure is one way to reduce resistance. (Flynn, Akashige, & Theodore, 2019). This can be accomplished by providing a longer surface or adding extra material with varied geometries into the enclosure's route. The addition of a longer surface or substance, on the other hand, increases the pressure drop over the collector. (Akpınar & Koçyiğit, 2010). This was also presented by Singh Yadav & Kumar Thapak (2014), where the surface roughness enhances flow turbulence and hence heat transfer efficiency. The thermal-hydraulic performance of the roughness geometry 'V-down rib with a gap' has been studied, and artificial roughness geometries utilized in solar air heater ducts have been reported. In comparison to a smooth duct, artificial roughness as an inherent element of the SAH module improves the thermos-

hydraulic performance of the system. (Singh, Chander, & Saini, 2015). The roughness of the absorber plate increases the heat transfer coefficient by increasing the friction coefficient, according to the findings by Lingayat, Chandramohan, & Raju, (2018).

According to Vyas & Punjabi (2014), the thermal efficiency and temperature gradient of three different flat plate air collector designs (plane absorber, transverse V-porous ribs, and inclined V-porous ribs of absorber) were evaluated in an experimental setting using solar radiation and natural convection flow models. These three models had a total thermal performance of 14.91 percent, 17.24 percent, and 20.04 percent, respectively. Additionally, greater system productivities indicated a decrease in the temperature gradient.

Naphon (2005) calculated the thermal performance of a longitudinally finned absorber plate solar air heater with a single glass cover to be around 60% at mass flow rates ranging from 0.02 kg/s to 0.1 kg/s. Additionally, increasing the fin height and number of fins decreases the rate of entropy generation while increasing thermal efficiency. Kumar & Chand (2017) expected that the longitudinal herringbone corrugated ultrafine solar air heater will improve its thermal performance. According to the findings, thermal efficiency improves as mass flow rate, solar radiation, and fin pitch and spacing decrease. Singh & Dhiman (2016) used an analytical model to predict the thermal performance of a longitudinally finned solar air heater and show how mass flow rate, recycle ratio, number of fins, and collector width affect thermal performance. For five numbers of fins, the minimum width of the collector is 0.3 m, the recycle ratio is 1.5, and the mass flow rate is 0.025 kg/s, the maximum thermal efficiency is found to be around 82 percent.

Priyam & Chand (2016) shows the influence of fin spacing and mass flow rate on a wavy finned solar air heater. The offset staggered finned solar air heater's thermal and thermohydraulic efficiencies are expected by Rai, Chand, & Sharma (2017). With a

reduction in fin spacing and an increase in fin height, the greatest percentage improvement in thermal and thermohydraulic efficiency is 114.1 percent and 112.65 percent, respectively. (Rai, Chand, & & Sharma, 2017).

Singh & Dhiman (2015) estimates that a solar air heater with double pass recycles and glass covers will have a thermal efficiency of around 79 percent. Solar power, on the other hand, the maximum number of fins feasible in an air heater is examined. It is recommended that 22 fins with a thickness of 1 mm be employed for improved thermal efficiency. The effect of cylindrical fins attached to the absorber plate on the solar air heater has been studied. In comparison to a basic predictable device, the findings reveal that properly allocating fins increase the output air temperature and thermal efficiency. (Gopi, 2014).

Koundinya & Krishnan (2014) presented a finned heat pipe with a solar module. The solar module's maximum temperature drop was determined to be 20°C using CFD calculations. Elsafi and Gandhidasan (2015) developed a mathematical model to predict the performance of a photovoltaic/thermal system with various fin configurations. The simulation findings indicated that adding a cooling fin to the PV/T system improved its performance. Taieb, Mohamed, and Driss (2016) employed a two-dimensional (2D) numerical simulation to determine the length of the internal fins in the PV-PCM system. The fins were useful in lowering the PV temperature increase. Additionally, the PV module was better cooled due to the fins' lengths of 25, 30, and 25 mm. Ibtisam (2018) provided a theoretical and practical examination of the cooling strategy that utilises fins attached to the rear side of the photovoltaic panel. According to the data, the fins reduced the temperature of the photovoltaic panel by around 5.7 percent.

2.3 Previous Studies about the effect of fins on solar collectors.

Based on the previous studies, some comparisons can be made about the effect of fins on solar collectors.

2.3.1 Fins Arrangement in Double Pass Solar Collector.

Increase the solar air heater's thermal performance by making use of fluid -structure interactions. One wonderful impact of the converging segment is that the converging segment may greatly boost the air velocity. Therefore, the usage of the sixteen converging cross fins toward the flow along the 0.75 m length has led to a comparable concept. The eight numbers of fins are affixed to the bottom of the absorber and backplates, each with the same number. Eight cross-sectional converging portions are therefore periodically formed. To analyze, the influence of air velocity on thermohydraulic performance the angle of fins is varied from 30 to 90 degrees. The objective is to boost the convective heat transfer to promote forced convective convection by raising the speed of the fluid. The convective heat transmission is dependent mostly on on-air velocity. Thus, sixteen fine numbers slanted at an angle of around 30 degrees, 60 degrees, and 90 degrees are employed to speed up fluxes and to pick the best air to provide the maximum thermohydraulic performance. In the same connection, fins are modified to show the effect and to create the optimal configuration. the hydraulic diameter of the fins. (Singh S., 2020).

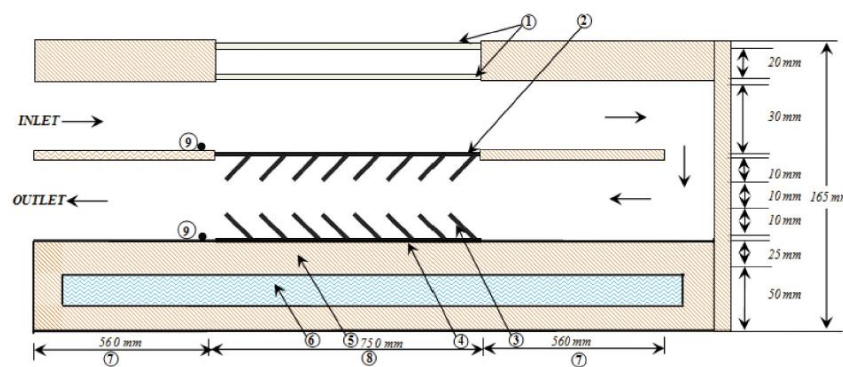


Figure. 2.2. Schematic Diagram of Experimental Setup. (Singh S., 2020).

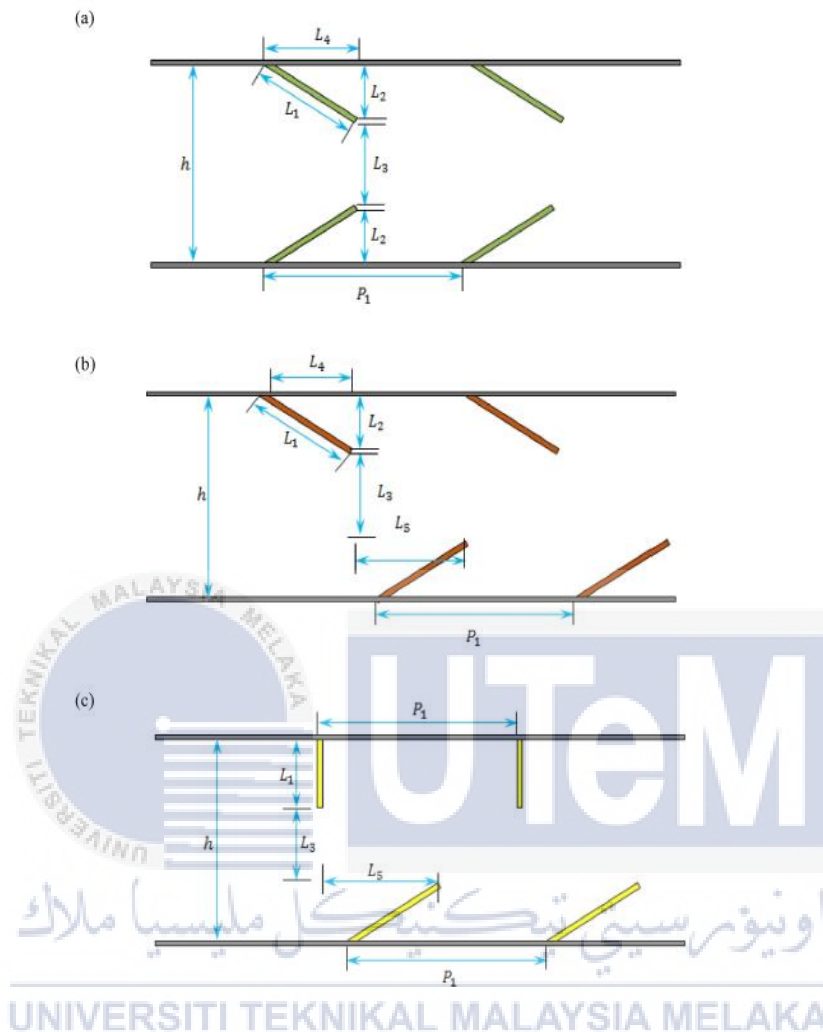


Figure. 2.3. Details of fins arrangements (a) in-line, (b) staggered, and (c) hybrid staggered. (Singh, 2020).

Figure. 2.3 details the shifting geometric characteristics and Table. 2.1 shows the parameters. The fins are employed to prevent thermal degradation and to promote convective heat transfer to the air to avoid high conductive material and thickness of 1 mm. The heat may be efficiently shared with fins by an absorbent air jet from the converging/narrow transverse section that helps to extract heat effectively and can result in high heat transfer to the air. When the thermal radiation is adjusted to the absorber plate, the finned rear plate is absorbed and heated the air. Findings on the rear plates will more interestingly lead the

flowing air to the absorber plate, which will greatly boost the air-to-fine absorber plate convective coefficient. (Singh S., 2020).

Table. 2.1. Design and operation parameters used in experimental work. (Singh S., 2020).

Heater dimensions			
Length of solar air heater, L		0.75 m	
Width of solar air heater, W		0.45 m	
Distance between glass covers, d_g		0.02 m	
Depth of the second channel, d_p		0.03 m	
Depth of the third channel, d_b		0.03 m	
Number of fin, n		16 (eight each on top and bottom plates)	
Thickness of absorber plate/back plate/fin, $t_{a/b/f}$		0.001 m	
Thickness of glass cover, t_g		0.004 m	
Insulation type		Glass wool	
Casing material		Softwood	
Fin length		0.014 m	
Fin Angle		30°	
Fin width		0.001 m	
Units and resolution of instrumentation			
Parameters	Range	Resolution	Accuracy
Thermocouples	0-400 °C	1 °C	± 1.0 °C
Pyranometer	0-2000 W/m ²	0.1 W/m ²	± 10 W/m ²
Anemometer	0-30 m/s	0.1 m/s	± 5%
Digital Micro manometer	± 4000 KPa	± 1 Pa	± 1%
Uncertainty in measurement			
Mass flow rate, \dot{m} (kg/s)	± 0.003		
Thermal efficiency, η (%)	± 0.15		

Thermal improvement findings are thus being used in the research to determine how to minimize the hydraulic diameter of the solar air heater conduit. The air is trapped in the closed channel between the glass covers, thereby reducing the surrounding area's heat losses. The closed channel's poor thermal conductivity and limited heat transfer contribute to the reduction of thermal losses in its environment. Additionally, the use of two glass covers helps to reduce radiation loss to the environment by collecting short wavelength radiation from the absorber plate, raising the temperature, and sharing that radiation with the circulating air via convective heat transfer. The double air route and increased air velocity in the periodic

converging sections extract more thermal energy from the solar heater elements on the solar air heater, lowering the element temperature and minimizing radiation losses in the surrounding. (Singh S., 2020).

According to Singh (2020), the research paper considered the thermal performance of the transverse finned absorber plate solar air heater was experimentally and numerically evaluated. The experimental study compares the thermal performance of single and double air pass operations for mass flow rates ranging from 0.01 to 0.04 kg/s. Fins with a 30-degree angle and a total of sixteen are examined, with eight on the down and top sides of the absorber and backplates, respectively. (Singh S., 2020).

As shown in Figure. 2.3, The angle, pitch, height, length, configurations such as inline, staggered, hybrid, and duct hydraulic diameter all have a quantitative effect on thermohydraulic performance as a function of Reynolds number. Additionally, CFD analysis is used to optimize the transverse finned solar air heater's geometrical and flow features. A Reynolds number between 3000 and 20000 is considered. The CFD results demonstrated the physics of fluid-structure interaction over the analyzed range of geometrical and flow parameters, hence assisting in the enhancement of the transverse finned solar air heater's thermal performance. (Singh S., 2020).

2.3.2 Fin and Baffle Configuration

As for AFSHARI, et al (2019), in their research, fins, and baffles with various geometrical porosity (holes) have been utilized in solar collectors, and their numerical influence on collector efficiency has been explored. As shown in Figure 2.4, in all solar collectors, the absorber plate is situated at the top of the collection, underneath the glass cover. In addition, baffles and fins have been added to the absorber plate's bottom.

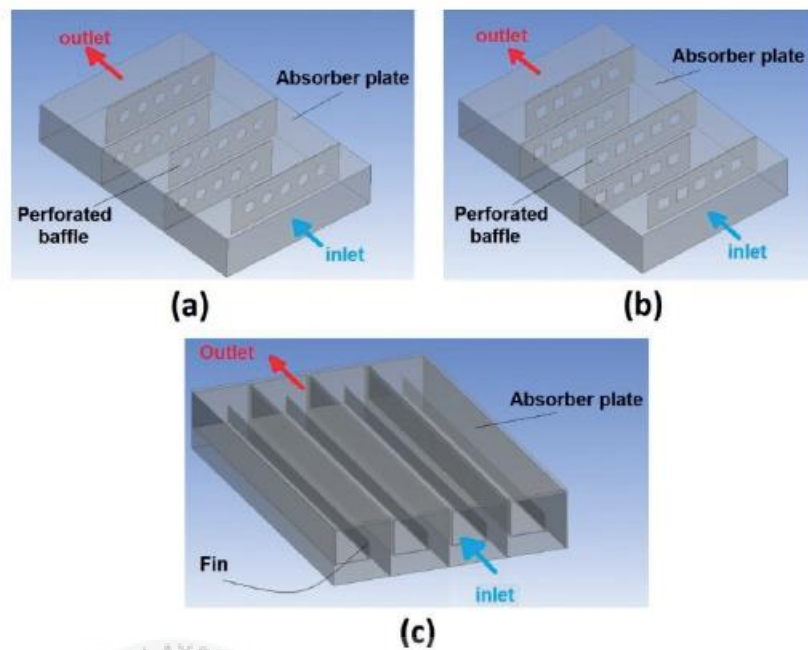


Figure 2.4. 3D Models of Solar Collectors. (AFSHARI, et al., 2019).

Perforated baffles were added to the absorber plate in two solar collectors (Figure 2.4. (a), Figure. 2.4(b)). In perforated baffles, two various pores were used, including rectangular and circular pores. The fins inserted into the absorber plate of the collection in the third solar collector, different from the other two collectors (Figure 2.4. (c)). The mesh generation of the collectors was conducted in the Ansys Fluent Mesh sub-program after solar collector shapes were generated. Figure. 2.5 shows the meshes generated for solar collectors. (AFSHARI, et al., 2019).

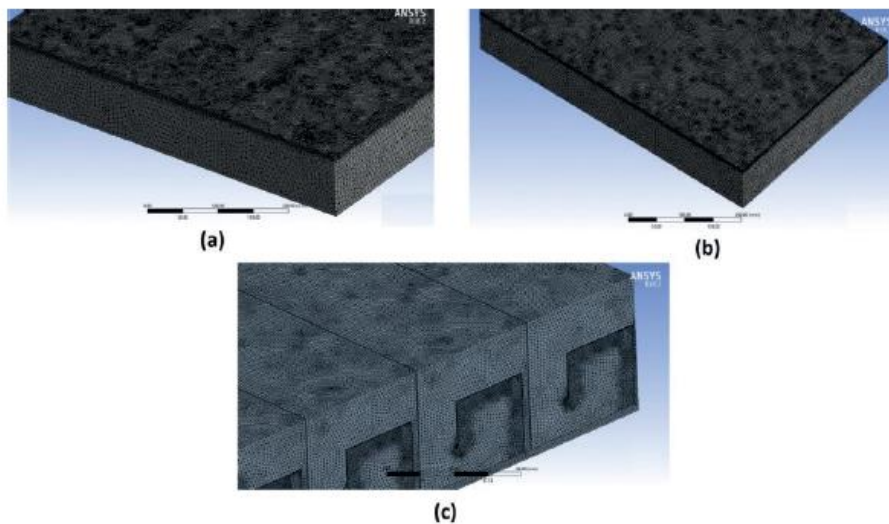


Figure. 2.5. Meshed view of solar collectors. (AFSHARI, et al., 2019).

The finer mesh structure is used in areas around the absorber plate, perforated baffles, and fins, as can be shown in Figure. 2.5 to make more precise findings. The highest values of skewness for created meshes are between 0.83 and 0.86 for three solar collectors. At the same time, average values of skewness are within 0.21-0.25 for produced meshes. (AFSHARI, et al., 2019).

UNIVERSITI TEKNIKAL MALAYSIA MELAKA

2.3.3 V-Groove Solar Air Collector

This article presents the results of a performance study on a v-groove solar air collector for drying applications. Experimental evidence indicates that a v-corrugated collector is more efficient at transferring heat than a flat plate collector. The effects of operating variables on thermal performance were investigated. The results demonstrate that increasing the flow rate results in a decrease in the temperature of the fluid entering the collector, resulting in an increase in efficiency due to lower thermal losses to the environment. These changes become less significant at a given flow rate. (Karim & Hawlader, 2005).

Solar drying's economics are highly dependent on the design of effective and adequate air collectors. Solar dryers with flat plate collectors make up the majority of solar dryers. The heat transfer coefficient of a surface in contact with air is much less than that of a surface in contact with water. Thus, while the size of the wall–water contact is a secondary factor in the design of solar water collectors, it is the key one in the design of solar air collectors. The fundamental disadvantage of flat plate air collectors is their low heat transfer coefficient, which results in inefficient thermal performance. If the accessible area for heat transmission is less than the intended area of the absorber, the absorber becomes overly hot, resulting in greater heat loss. (Karim & Hawlader, 2005).

Figure. 2.6 illustrates the detailed configuration of the collector used in this study. Although the collector was intended for single- and double-pass operation, this study discusses solely the findings of single-pass operation. Air was pulled into the back plenum and flowed through the passage between the absorber and backplate for single-pass operation. Perforated sheets were utilized in the front and back plenums to disperse the flowing air uniformly across the collection channel. The bottom of the v-groove was resting on the collector's backplate. (Karim & Hawlader, 2005).

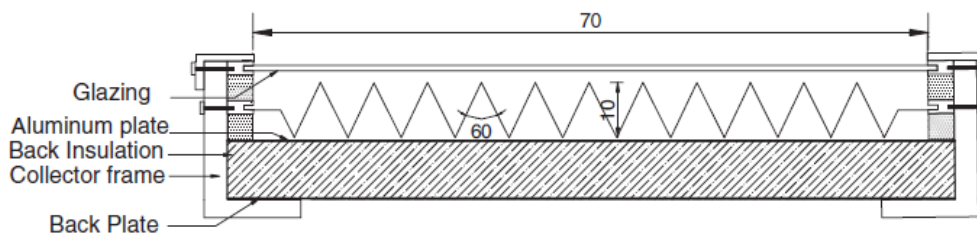


Figure. 2.6. Cross-Sectional View of v-groove. (Karim & Hawlader, 2005).

2.3.4 Flat Plate Solar Collector Performance Assessment with Internal Fins and Porous Media.

The work is concerned with the numerical simulation and experimental examination of a flat internal geometry plate with fins and porous media. The findings of these tests are compared to experimental data in order to gain a better understanding of the CFD simulations' exact nature. ANSYS Fluent is used for the CFD analysis. A mesh sensitivity test is performed on cells with four dimensions, and a mesh independence test is performed on cells with no dimensions. During CFD analysis, $k - \epsilon$ turbulence models are employed to simulate the physical circumstances of the experiment. (Kansara, Pathak, & Patel, 2021).

The experimental setup will be used to evaluate and validate the geometry's performance. One of the primary objectives of this study is to avoid modifications in the collector's external major dimensions. It is tested using a solar simulator. The air is assumed to flow freely in this investigation. The mass air flow rate and heat flow are the variables in the proposed survey. The working fluid is utilized to transfer energy from the heat absorber plate to the electrical circuit. The temperature increase of the air via the collector, the amount of heat absorbed by the air, and the decrease in air pressure across the channel are used to determine performance. Furthermore, the present work examines the effect of polished and porous medium qualities. Additionally, this study looks at the three distinct arrangements. The following explanation differentiates between cases 1 (empty collector), 2 (inner longitudinal fin), and 3 (porous metal foam collector). (Kansara, Pathak, & Patel, 2021).

SolidWorks design modeling and fluent analyses of ANSYS are used for this inquiry. The computer field explored in this work is represented in Figure. 2.7. The domain includes walls of enclosures, plate absorbing, fin/porous medium, intake, and output. (Kansara, Pathak, & Patel, 2021).

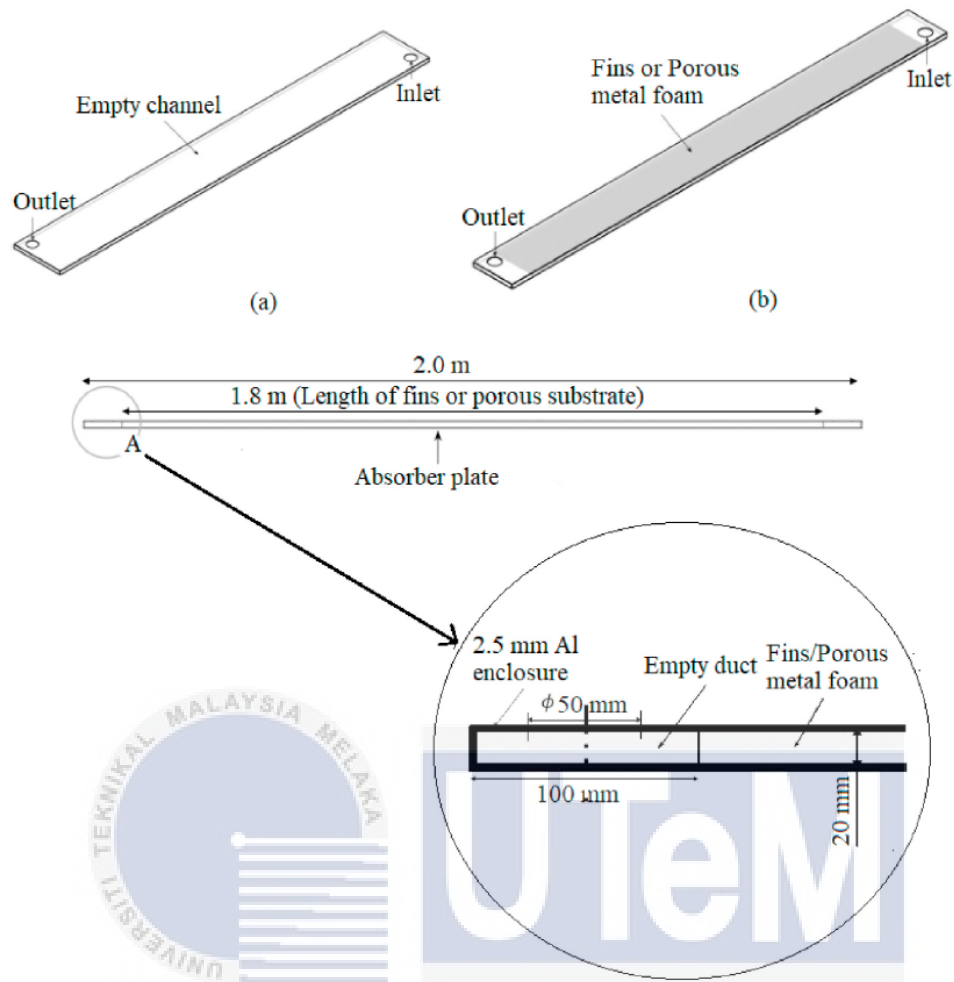


Figure. 2.7. Schematic Diagram of flat plate collectors. (Kansara, Pathak, & Patel, 2021).

At first, a tetrahedral mesh is made and afterward converted into a polyhedral mesh. The cell sizes 5 mm, 4 mm, 3 mm, and 2.5 mm are utilized for grid independence testing. The mesh size is almost consistent across the geometry to maximize solutions except for the entrance and exit when the closeness and the curvature criteria are close. The GCI approach is used to identify the CFD analysis's discretization error. (Roache, 1998). The observable parameter is set to the temperature of the air exit. The information in Table. 2.2 is shown for each mesh scenario. (Kansara, Pathak, & Patel, 2021).

Table. 2.2. Mesh information of the computational model. (Kansara, Pathak, & Patel, 2021).

Case	Cell size (mm)	Number of elements	Growth rate
Case 1: collector with empty channel	5	21239	1.4
	4	110122	1.4
	3	412402	1.4, 1.2
	2.5	843149	1.4, 1.2
Case 2: collector with internal fins	5	381990	1.4
	4	442746	1.4
	3	749626	1.4, 1.2
	2.5	1004480	1.4, 1.2
Case 3: collector filled with porous metal foam	5	174765	1.4
	4	283537	1.4
	3	539734	1.4, 1.2
	2.5	1013533	1.4, 1.2

All three situations were assessed mesh-independently using four different mesh sizes. For each mesh configuration, similar boundary conditions and solver methodologies were used to achieve comparable results. There are four different sizes available: 5, 4, 3, and 2.5 mm. They are available on a standard basis. The mesh is initially totally tetrahedral and is then converted to polyhedral and hexahedral shapes using ANSYS Fluent. Apart from the entrance, outflow, and border of the amortizes, the mesh is improved. Indoor experiments on two collectors are conducted to validate and precisely determine the CFD model (empty or fin geometry). By utilizing a non-commercial, self-designed solar simulator, the risk of continuously changing conditions such as wind speed, solar radiation, or daylight time can be minimized. There are 16 infrared (IR) bulbs in place in this solar simulator, which are organized in a 4×4 matrix range. The IR light details are as illustrated in Table. 2.3. (Kansara, Pathak, & Patel, 2021).

Table. 2.3. Specification of IR lamp. (Kansara, Pathak, & Patel, 2021).

Product name	Half-white heating lamp
Tube diameter	ϕ 10 mm
Total length	500 mm
Voltage	220 V
Power	1000 W
Ceramic	SK15
Wire length	250 mm

A solar circuit is designed in such a way that each control switch can power a specific number of bulbs, allowing for variable irradiation flows in the solar simulator. The collector and simulator are maintained horizontally. As seen in figures 2.8 and 2.9 are a schematic diagram and experimental installation. (Kansara, Pathak, & Patel, 2021).

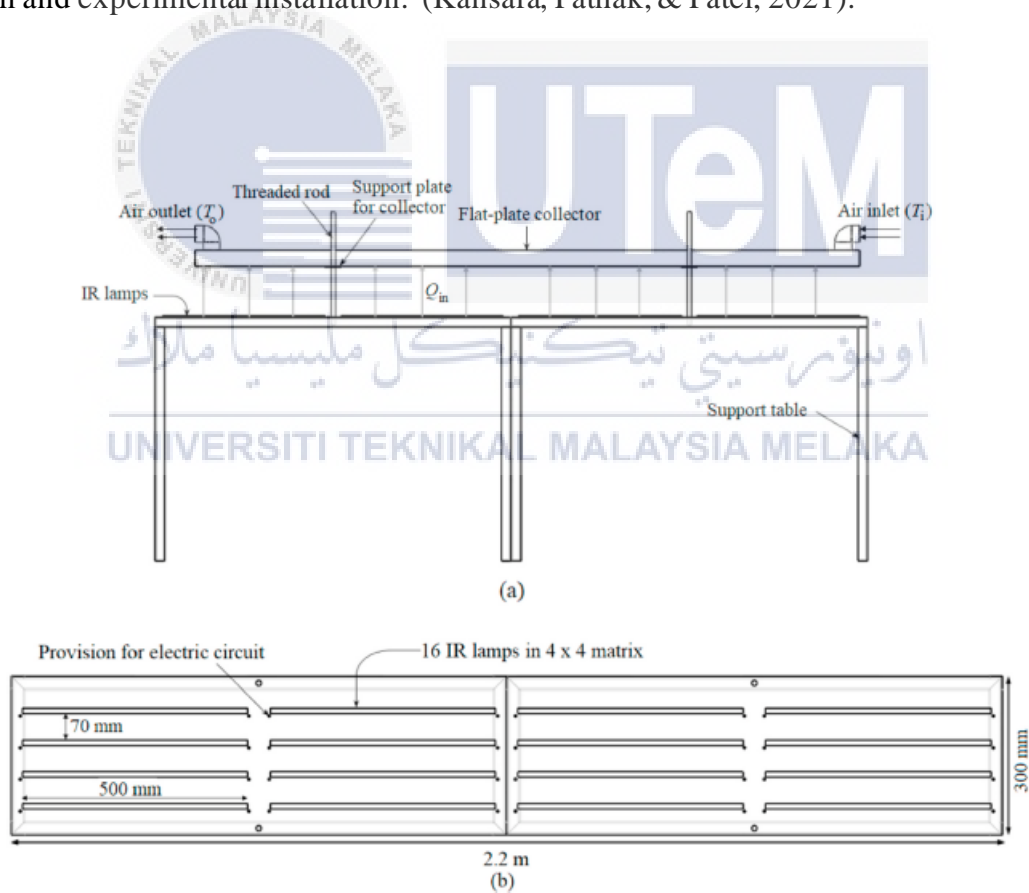
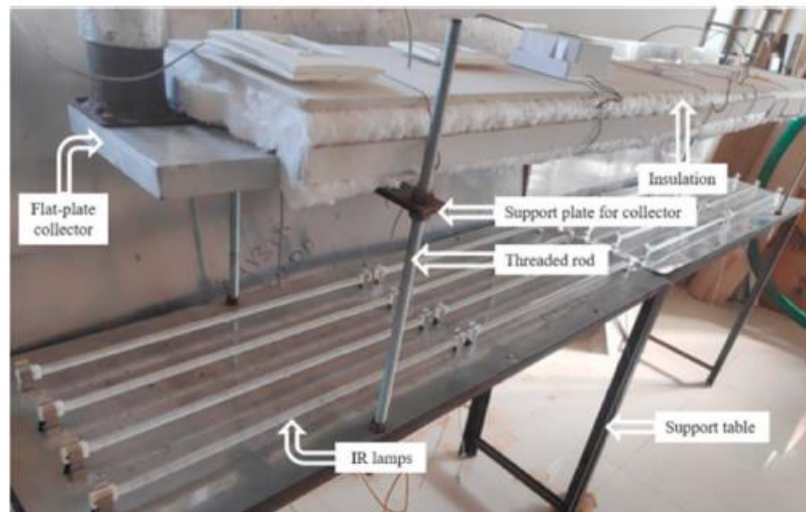


Figure. 2.8. Diagrammatic representation of (a) a solar simulator and (b) the dimensions of an infrared lamp and array layout. (Kansara, Pathak, & Patel, 2021).



(a)



(b)

Figure. 2.9. Experimental setups (a) layout (b) under operating conditions. (Kansara, Pathak, & Patel, 2021).

2.3.5 Effect of fin pattern on the air-side performance of herringbone wavy fin-and-tube heat exchangers

The article gives fresh experimental data on the air-side performance of fin-and-tube heat exchangers with herringbone wavy fin configurations. Unlike the majority of previous research, the current trials focused on the effect of fin designs and edge corrugations on the air-side performance of heat exchangers. The experimental setup is primarily formed of an insulated open wind tunnel and herringbone wavy fin-and-tube heat exchangers made of aluminium tubes with wavy fins. Two distinct types of wavy fin patterns are discussed, both of which are frequently employed in the industry. Operating fluids are air and hot water on the airside and tube side, respectively. The experimental results indicate that the fin pattern has a significant influence on heat transfer and flow characteristics. Wavy fin and tube heat exchangers are fairly common types of plate-fin and tube heat exchangers that can be found in a wide number of industrial applications. The thermal resistance of the heat exchanger's airside often limits heat transfer in these applications. The airside heat transmission is improved by altering the fin configuration of the heat exchanger. Due to the increased surface area and improved airflow mixing that herringbone wavy-fin corrugation provides, it is increasingly widely used. (Chokeman & Wongwises, 2005).

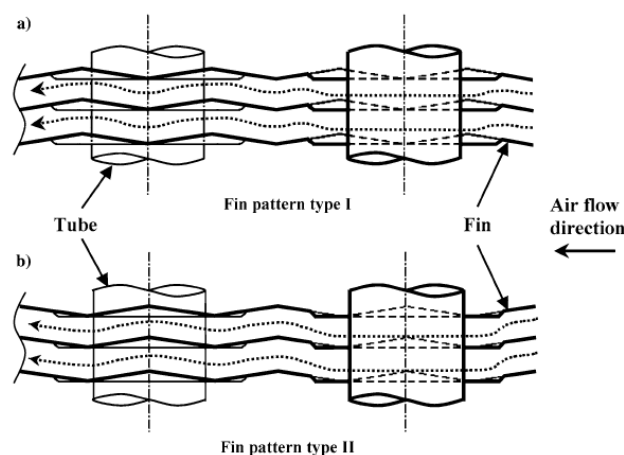


Figure. 2.10. The corrugated flow channel inside the heat exchanger with the wavy fin design type I and type II is depicted schematically. (Chokeman & Wongwises, 2005).

2.3.6 Operative Parameters and Thermal Efficiency of Solar Collector Effect Of Fins Attachment.

The proposed solar collectors are made in a laboratory in another research work by Daliran & Ajabshirchi (2018) with a total surface area of 1 m², in two types of C1 (no fin) and C2 (finned). A panel having a sun channel of fins, a glass cover, an absorber plate, a backside panel, fins, and a thermal insulator are shown in Figure. 2.11 (a). The 0.03 meters thick standard glass cover, consisting of a conventional 0.00115 meters thick iron sheet, is installed at a distance of 0.03 meters from the absorber plate. In addition, the distance between the absorber plate and the rear board is 0.04 m, comparable to the air channel height. The rectangular galvanized fins on the air channel of C1 with 5 x 4 cm² surfaces and 0.6 mm thickness are united by an angle of 45 degrees into a backboard with 125.5 x 81 cm² surface sizes and a thickness of 8 mm.

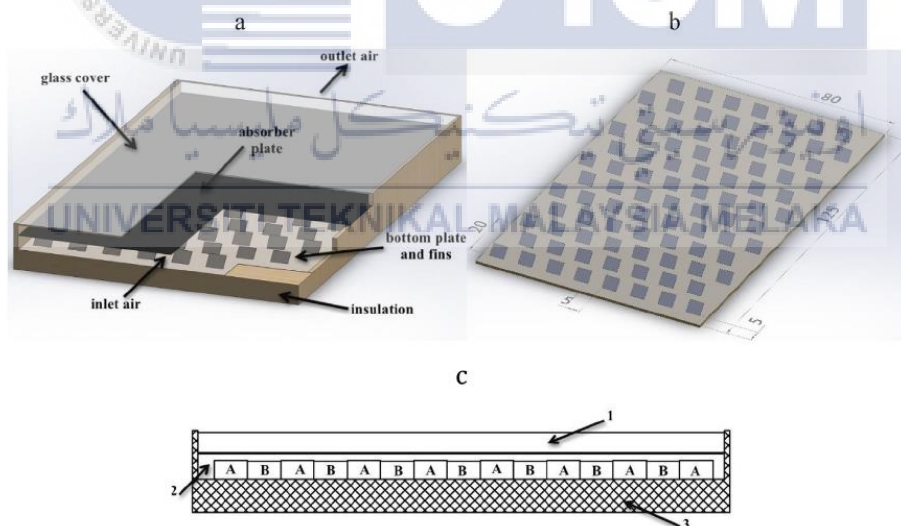


Figure. 2.11. (a) Main parts of collector type C1, (b) fins configuration on the backboard, (c) front view of the suitable overlap for the two fin groups (A: first row fins, B: second-row fins). 1: The space between the glass cover and absorber plate, 2: air passage, 3: stone wool insulator. (Daliran & Ajabshirchi, 2018).

The lateral distances between the borders of each of the neighboring fins and the longitudinal distance between them are 5 cm and 20 cm. The distance from the front and side edges of the back of the first-row fins is set at 5 and 2.5 cm. Fins are arranged across the rear board in Figure. 2.11 (b). The fins were placed in two forms to preserve enough overlap: form A, which consisted of six rows of eight fins apiece, and form B, which consisted of six rows of seven fins. This appropriate overlap may be seen in rows A and B of Figure. 2.11 (c). A 0.05 m-thick stone wool insulator is utilized to reduce heat losses from the collector's back end. Then, to improve collector part deployment, a 0.016m thick MDF framework is used. (Daliran & Ajabshirchi, 2018).

2.4 The Effect Of Fins

The length, height, pitch, and fin angle affect the thermal performance in a solar collector. A staggered, inline, or hybrid fins arrangement also affects the performance. The Nusselt number and the friction factor are affected by such arrangements of fins in the design. Whether the fins arrangement will be in a staggered, inline, or hybrid also affects the performance especially the thermohydraulic performance parameter (THPP). For inline configuration, the THPP decreases with the increase of Renault number for all fin lengths as in such configuration, high-pressure drop occurs. As for staggered configuration, there is increment when compared to the inline configuration which shows the advantage of using staggered configuration over inline. (Singh, 2020).

When using the hybrid configuration, it is noted that the increase in hydraulic diameter presents improvement in THPP. Hybrid staggered configuration means high heat transfer due to the high value of the Nusselt number. (Singh, 2020).

When measuring outlet temperature in all collectors of different designs, the outlet temperature in fin integrated solar collector is higher in all air velocities in comparison to others. Integrating fins to the absorber plate will make the ways narrower which decreases the air velocity thus gain more thermal energy by flowing air. (AFSHARI, et al., 2019).

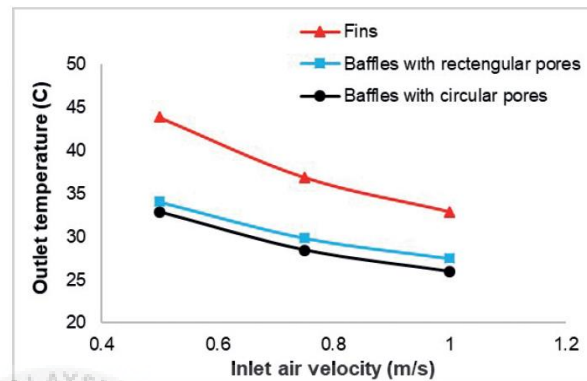


Figure. 2.12. Variation of Collector Outlet Temperature Via Inlet Air Velocity. (AFSHARI, et al., 2019).

A collector with v-grooves is 13% more efficient than one with flat plates. The efficiency of the collector is strongly reliant on the airflow rate. The efficiency increased from 0.41 at 0.01 of 0.035 kg/m²s to 0.71 at 0.054 of 0.035 kg/m²s. As efficiency increased in proportion to flow rate, the output temperature decreased correspondingly. Due to the high efficiency and outlet temperature requirements for the majority of agricultural drying applications, a flow rate of 0.035 kg/m²s is considered appropriate for this collector configuration. The collector's temperature increase equation is deduced. This equation is considered useful for calculating the output temperature from known meteorological data, which enables the design of collectors for a number of purposes. (Karim & Hawlader, 2005).

The temperature and warmth trend in other designs is similar, but the values are increased. As the surface between air and collection rises, the temperature rises rapidly. In addition, the connection of fins to the channel has greatly lowered flow unevenness and the

number of hot spots. As Figure. 2.12 shows, the number of fins also reduces thermal strength, leading to better air heat absorption. (Kansara, Pathak, & Patel, 2021).

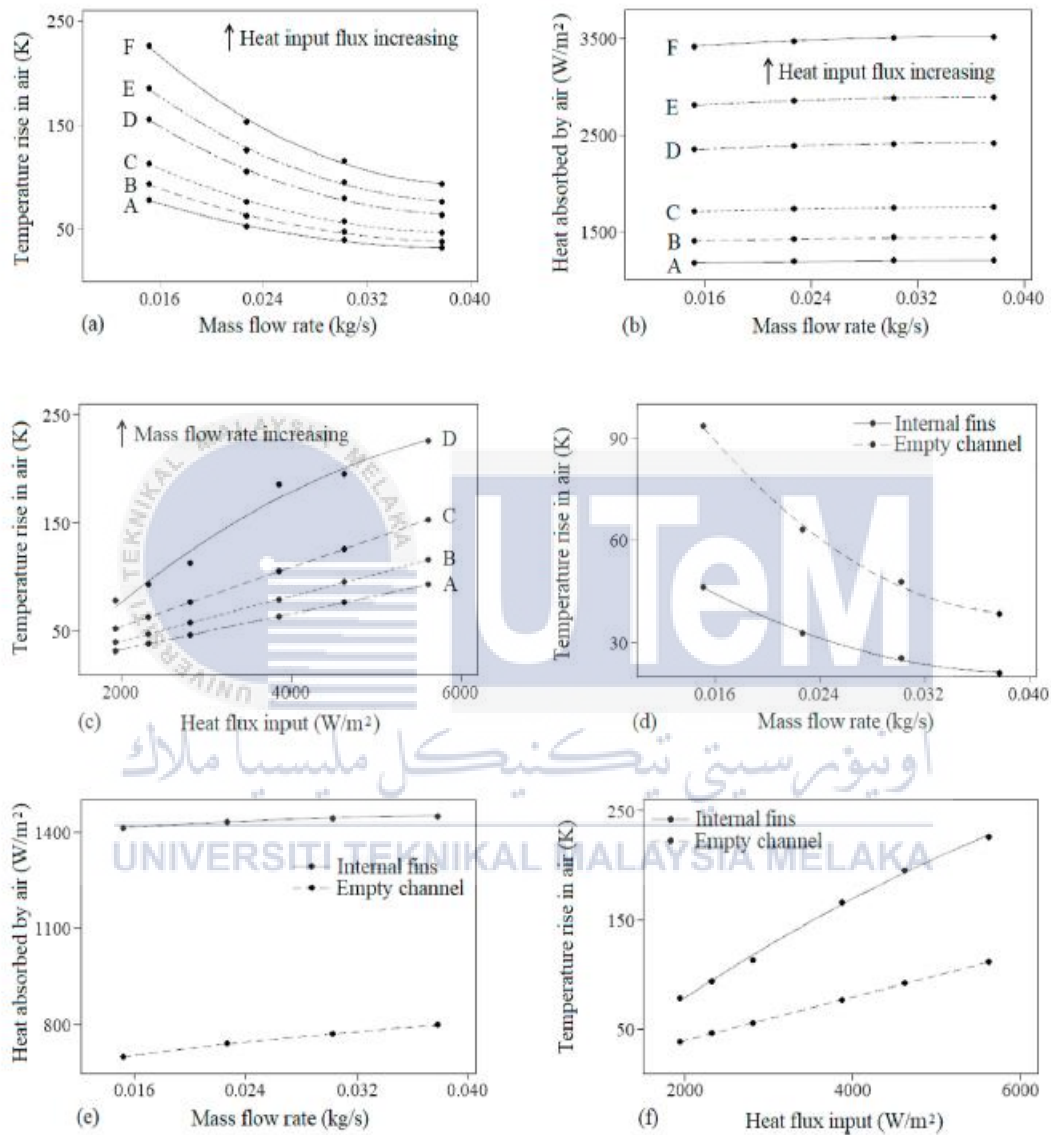


Figure 2.13. Variation of temperature rise and heat absorbed by air with mass flow rate and heat flux input ((a), (b), and (c) are for case-2; (d), (e), and (f) comparison between case-1 (no fins) and case-2 (with fins). (Kansara, Pathak, & Patel, 2021).

Table. 2.4. The number of fins and corresponding thermal resistance to the air. (Kansara, Pathak, & Patel, 2021).

Number of fins	10	15	20	25
Thermal resistance (K/W)	0.35	0.21	0.05	0.01

Figure 2.14 illustrates the influence of fin pattern on heat transfer coefficient and pressure drop in wavy fin-and-tube heat exchangers. As shown in this figure, the heat exchanger with the type II fin design has a higher heat transfer coefficient and a smaller pressure drop than the heat exchanger with the type I fin pattern. However, when the heat transfer coefficient and pressure drop of heat exchangers with fin pattern type II are compared to those with fin pattern type I, percentage increases of 5.25–15.39 percent and 0–6.61 percent, respectively, are seen. (Chokeman & Wongwises, 2005).

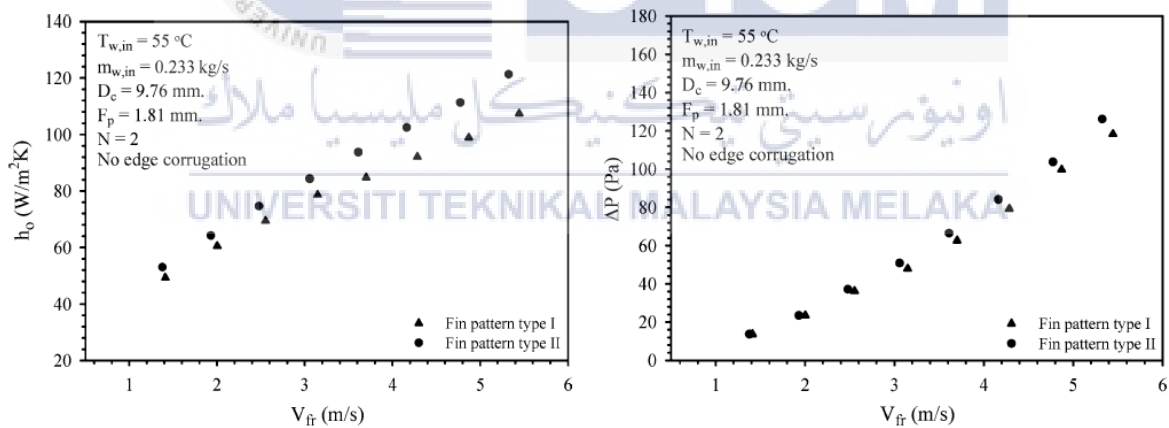


Figure. 2.14. Coefficient of heat transmission and pressure decrease. (Chokeman & Wongwises, 2005).

Apart from that, with a constant air volume flow in a solar flat plate collector, the hydraulic diameter, the number of Reynold, and the number of Nusselt all drop. The smaller hydraulic diameter benefited, while the number of Nusselt and Reynold dropped, increasing the heat transfer coefficient between the absorber plate and the liquid. (Daliran & Ajabshirchi, 2018).

In a conclusion, the length, height, pitch, and angle of the fins all affect the thermal performance of a solar collector. The fin pattern determines the nusselt number and friction factor, regardless of whether the fins are staggered, inline, or hybrid. Following that, by integrating fins onto the absorber plate, the routes narrow, lowering the air velocity and therefore capturing more thermal energy from the flowing air. Additionally, v-groove collectors are 13% more efficient than flat plate collectors. The collector's efficiency is highly dependent on the airflow rate. As efficiency grew in proportion to flow rate, the temperature at the output decreased proportionately. As a result, the requisite flow rate will be necessary. Additionally, when the surface area of the air between it and the collection increases, the temperature rises rapidly. Additionally, by connecting the fins to the channel, the flow is more evenly distributed and the number of hot spots is greatly reduced.

Chapter 3

METHODOLOGY

3.1 Introduction

In this chapter, the methodology and general strategy are discussed, and the research and experimental processes are explained with more precision. How the findings are acquired for CFD is given as the approach utilized in this research. This project begins with a study of Ansys Fluent software and learns how to create, draw and find the specific points to observe the results so that data for analysis is correct and legitimate. This report focuses on the computational and experimental analysis of a flat plate collector as internal geometry with and without fins. The findings are compared and assessed against the available current data to assess the correctness of CFD simulations.

3.2 Overview

This chapter is on double-pass flat collectors. The double-pass flat solar collector with and without fins. The solar collector has a fin on the absorber, a cover, a three-hole airflow backpack, and an insulator. (i) constant performance; (ii) constant thermal conductivity for fins and absorbers; (iv) uniform thermal gain along the collector's length to simplify the analysis. The simulation examines the impact of fins on solar collectors. This study uses air as a working fluid. The fluid circulates through passages heated by the thermal absorber plate. The performance parameter to be investigated is air temperature increase, velocity, and pressure decrease.

3.3 Methodology Chart

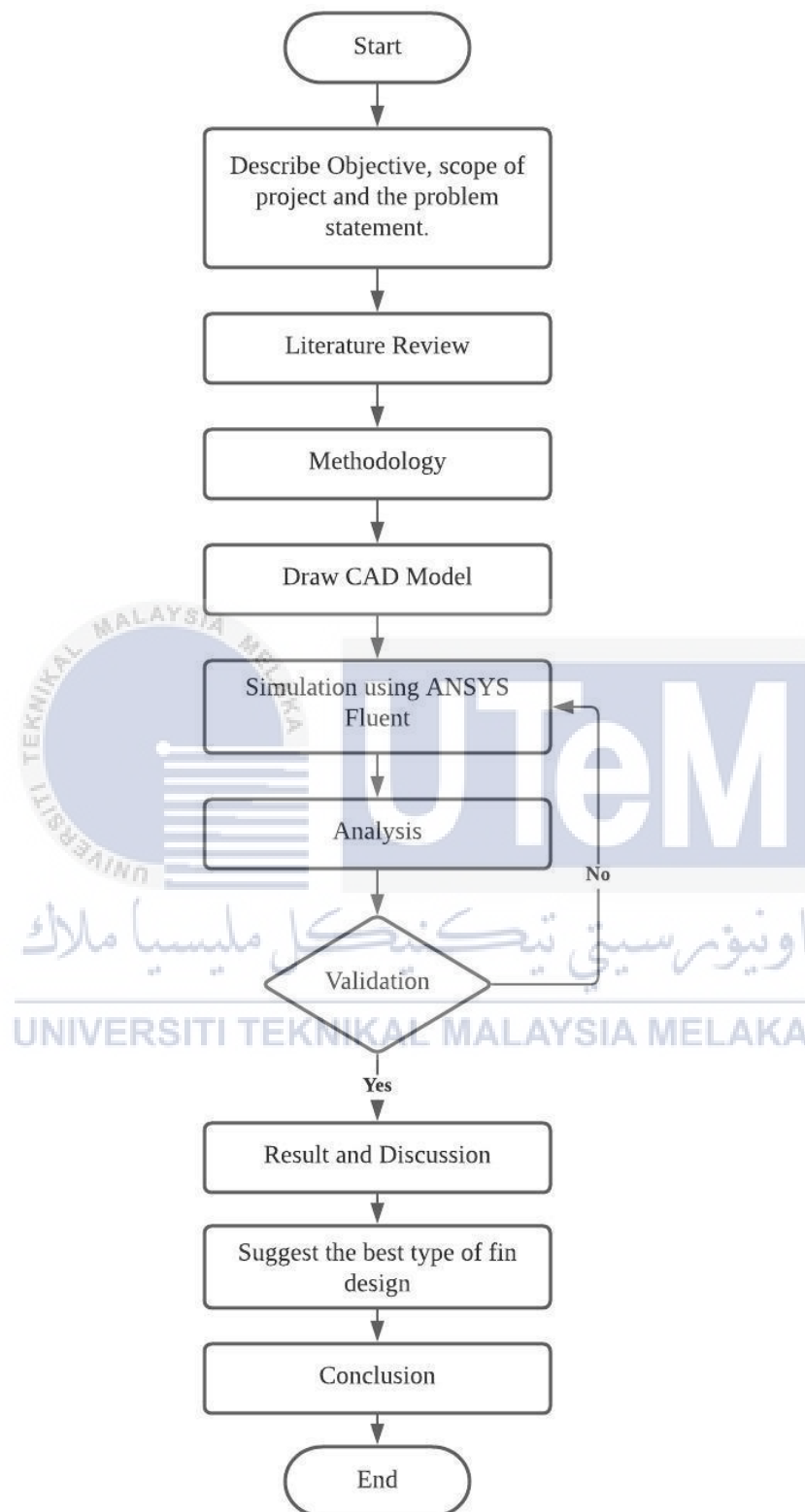


Figure. 3.1. Methodology Flow Chart

3.4 Simulation Procedures

3.4.1 Simulation Setup

A double-pass flat plate solar collector with fins was used in this study as shown in figure 3-2. The solar collector is equipped with an absorber plate with longitudinal fins arrangement. The setup of the CFD model of the study report. The investigation is carried out with Solidworks design modeling and ANSYS Fluent analysis. The schematic and 3D computational domains designed as the study model are shown in Figures 3-3 and 3-4. The domain is made up of enclosure walls, a fine absorber plate, a glass cover, an air inlet, and an air exit. Figure 3-4 illustrates the arrangement under the absorber plate of the longitudinal fins.

The appropriate tilt angle for each site will be established using the latitude of the area and the day of each location. As a result, it is advised that the appropriate tilt angle map for Malaysia be based on latitude. Solar sites are thus classified according to Malaysia's defined regions, which include Kuala Lumpur (Zone A), Johor Bharu (Zone B), Ipoh (Zone C), Kuching (Zone D), and Alor Setar (Zone E) (Zone E). The ideal wet season tilt angles for Kuala Lumpur, Johor Bahru, Ipoh, Kuching, and Alor Setar are 19° , 17° , 19° , 15° , and 23° , while the ideal dry season tilt angle is zero from April to September. (Khatib, Mohamed, Mahmoud, & Sopian, 2015).

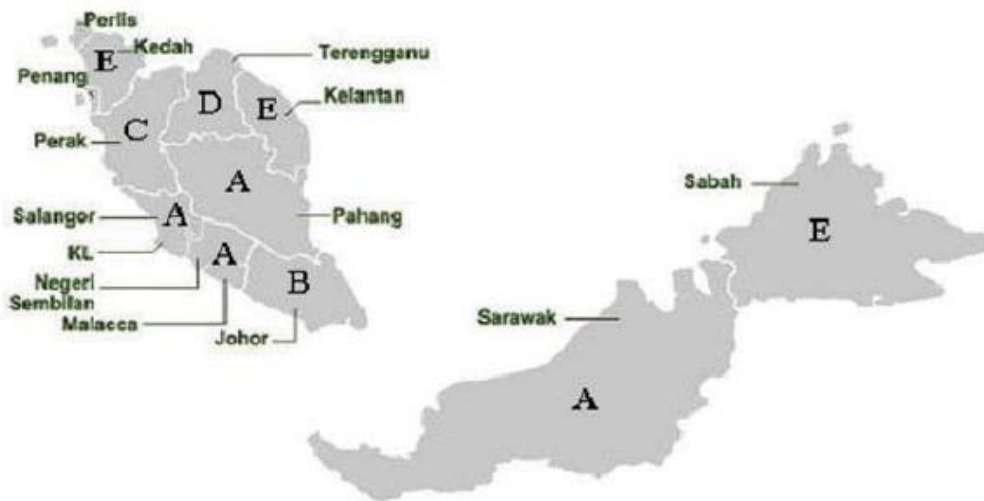


Figure 3.2. Zone for optimum angles. (Khatib, Mohamed, Mahmoud, & Sopian, 2015).

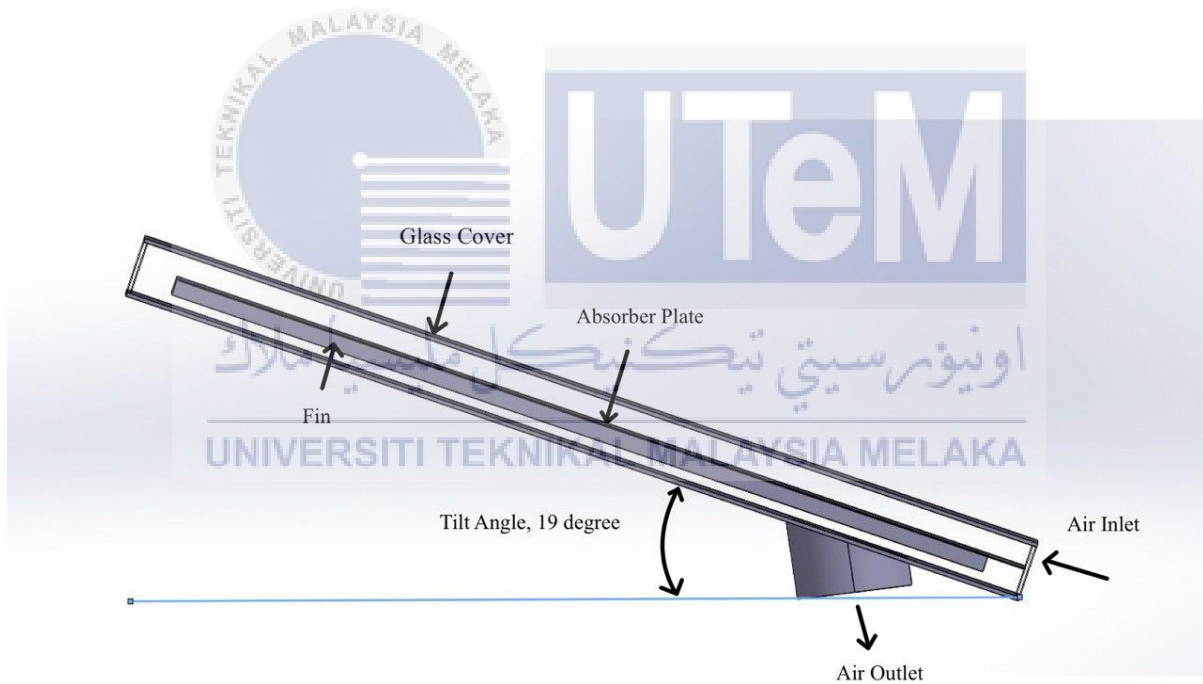


Figure 3.3. The schematic of a double-pass solar collector with fins absorber in the second channel.

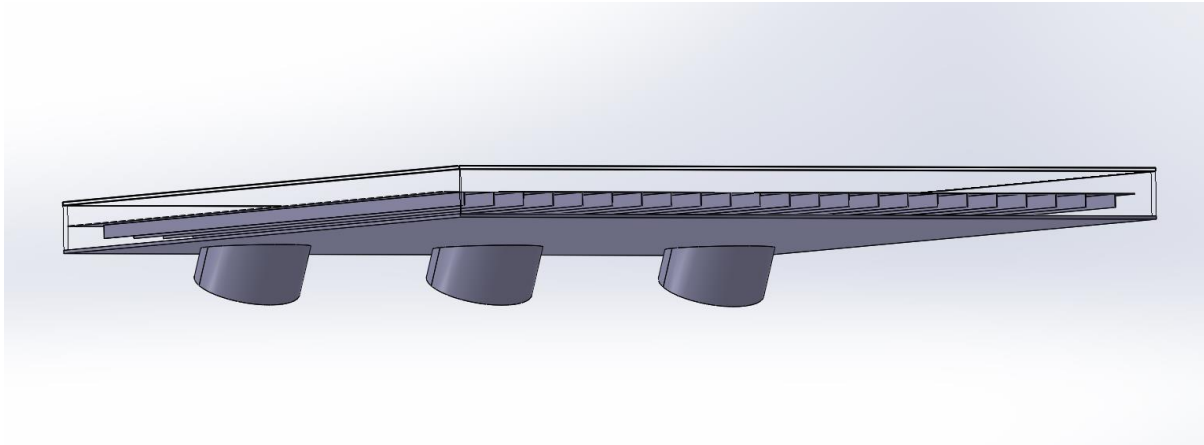


Figure. 3.4. Three-dimensional model of a double-pass solar collector with fins.



Figure. 3.5. Study Model in a solar drying system.

A 1200 mm x 1200 mm x 67 mm solar collector with a double pass. The collector is fitted with a 1 mm thick absorber plate. The plate has a length of 1095 mm with its

longitudinal fins. Every fin is 20 mm high and 1 mm thick. The fins are 50 mm apart. Each outlet has a radius of 80 mm.

3.4.2 Boundary Conditions for The Optimization Study:

- Inlet: Velocity inlet at 3.3 m/s
- Outlet: Pressure outlet
- Top wall (Glass): Constant wall flux
- Fin Surfaces: Constant wall flux
- Bottom wall: No-slip and zero temperature gradient (insulation)
- Sidewalls: No-slip and zero temperature gradients (insulation)
- Entry and exit section: No-slip and zero temperature gradient (insulation)

3.4.3 Numerical Method

The numerical methods and the simulation approach for this current study are presented in this subchapter.

- A Computational Fluid Dynamics (CFD) method using ANSYS Fluent software is implemented in this study.
- A pressure-based approach is employed in the model.
- The SIMPLE method is used to provide pressure-velocity coupling.
- The second-order upwind method is applied to discretize the convection terms.

- The density, viscosity, and thermal conductivity of the airflow are considered constant.
- The sky temperature changes, the wind velocity changes are abandoned during the simulation.

3.4.4 Meshing

The study produces a tetrahedral mesh. The cell mesh size is almost uniform across the geometry.

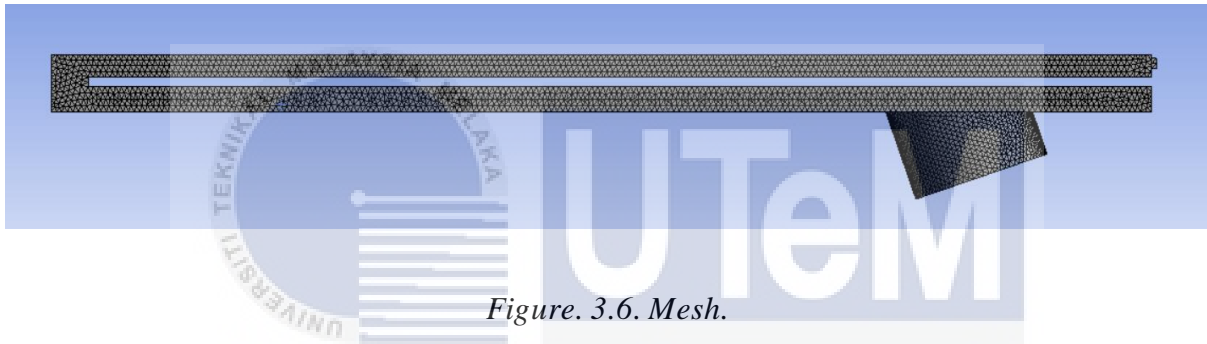


Figure. 3.6. Mesh.

On the working fluid, a patch conforming approach is used to generate a tetrahedral mesh. After the mesh is generated, it is examined to ensure that its quality is acceptable for producing dependable results in ANSYS Fluent. The average orthogonal quality of the meshed model with 549489 nodes and 2626916 elements is 0.76, while the average skewness is 0.23, according to the ANSYS Meshing Software. Based on the ANSYS Mesh quality recommendations, it can be inferred that the mesh quality of this model is adequate and that it may be used for simulation in ANSYS Fluent software.

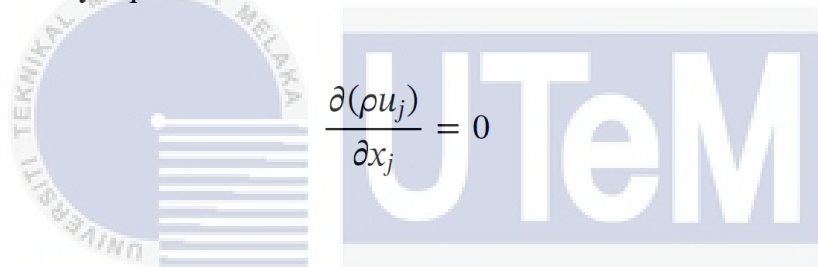
3.5 Governing Equation

Governing equation for fluid flow and heat transfer.

3.5.1 Fluid Flow

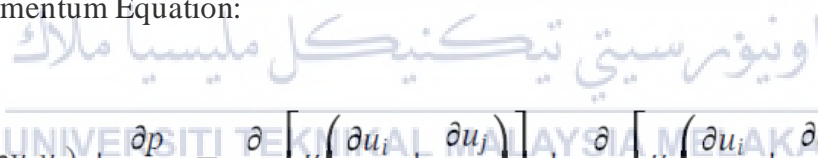
The study currently uses the program Ansys-Fluent to carry out constant-state numerical simulations. The program involves the solution of conservation equations, such as continuity, momentum, and energy stated in Equations (1) to (3), which imply the technique of finite volume. The following is given for conservation equations. (Kumar & Saini, 2009). (Yadav & Bhagoria, 2013).

Equation 1 Continuity Equation:



$$\frac{\partial(\rho u_j)}{\partial x_j} = 0$$

Equation 2 Momentum Equation:



$$\frac{\partial}{\partial x_j}(\rho u_i u_j) + \frac{\partial p}{\partial x_i} = \frac{\partial}{\partial x_j} \left[\mu \left(\frac{\partial u_i}{\partial x_j} + \frac{\partial u_j}{\partial x_i} \right) \right] + \frac{\partial}{\partial x_j} \left[\mu_t \left(\frac{\partial u_i}{\partial x_j} + \frac{\partial u_j}{\partial x_i} \right) \right]$$

Equation 3 Energy Equation:

$$\frac{\partial}{\partial x_i}(\rho u_j T) - \frac{\partial}{\partial x_j} \left[(\Gamma + \Gamma_t) \frac{\partial T}{\partial x_j} \right] = 0$$

Where $\Gamma_t = \mu_t/Pr$ is the turbulent thermal diffusivity, $\Gamma = \mu/Pr$ is the molecular thermal diffusivity, Pr is the Prandtl number, μ and μ_t is the viscosity (Ns/m²) and thermal viscosity,

respectively, ρ is the density, P is the pressure (Pascal), u is the velocity (m/s), and T is the temperature (K).

3.5.2 Heat Transfer

In this study, the solid material is supposed to be constantly thermal and may be seen as a thin wall. The needed space is estimated for the collector with fins.

Equation 4 Required space between fins:

$$b = \frac{W - N_{fin}t_{fin}}{N_{fin} - 1}$$

Where W is the width of the collector channel (mm), N is the number of fins and t is the thickness of fins.

Equation 5 Velocity between fins:

$$V = \frac{\dot{m}}{N_{fin} \cdot b \cdot H_f}$$

Where H_f the height of the fin.

Equation 6 Reynold number for air between fins:

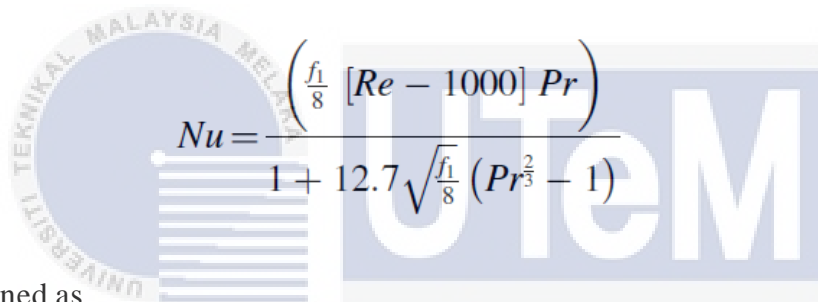
$$Re = \frac{\rho V b}{\mu} \frac{b}{L}$$

Where L is the length of the fin (mm).

Nusselt number is obtained through Gnielinski modified Petrichor Popov equation.

(Incropera & DeWitt, 1996) as given below:

Equation 7 Nusselt Number:



$$Nu = \frac{\left(\frac{f_1}{8} [Re - 1000] Pr\right)}{1 + 12.7 \sqrt{\frac{f_1}{8}} (Pr^{\frac{2}{3}} - 1)}$$

Where f is defined as

Equation 8 Definition of f:

$$f_1 = -6.38 \times 10^{-13} Re^3 + 1.17 \times 10^{-8} Re^2 - 6.69 \times 10^{-5} Re + 0.147$$

The heat transfer coefficient between fins is thus obtained by,

Equation 9 Heat Transfer coefficient:

$$h = Nu \frac{k_f}{b}$$

Where k_f is the thermal conductivity of the fluid. (W/mk).

For the outlet temperature of air from the collector, the basic equation of heat flux can be used.

Equation 10 Heat Flux:

$$Q = mC_p(T_o - T_i)$$

Where C_p is the constant pressure-specific heat. (J/kg.K).



Chapter 4

RESULTS AND ANALYSIS

4.1 Study Model Results

The two-phase solar thermal collector results were obtained by the collection of data from the study model. The measurements will be made of the flow, the fluid temperature inside the solar collector, and the outlet temperature.

4.1.1 Results of Double Phase Solar Collector with Fins

The design of the double phase thermal collector is based on a model that is equipped together in a solar drying system. The solar collector is equipped with straight fins under the absorber to improve the heat thermal efficiency of the solar collector.



Figure. 4.1. Solar Collector Study Model.

4.1.2 Flow Trajectories of Double Phase Solar Collector with Fins

The air will flow from outside into the inlet of the solar collector where it will flow on the absorber and enter the fins before going to the outlet. Figure 4.2 (a) shows the flow trajectories of the solar collector. Figure 4.2 (b) shows how the air flows under the absorber towards the three outlets.

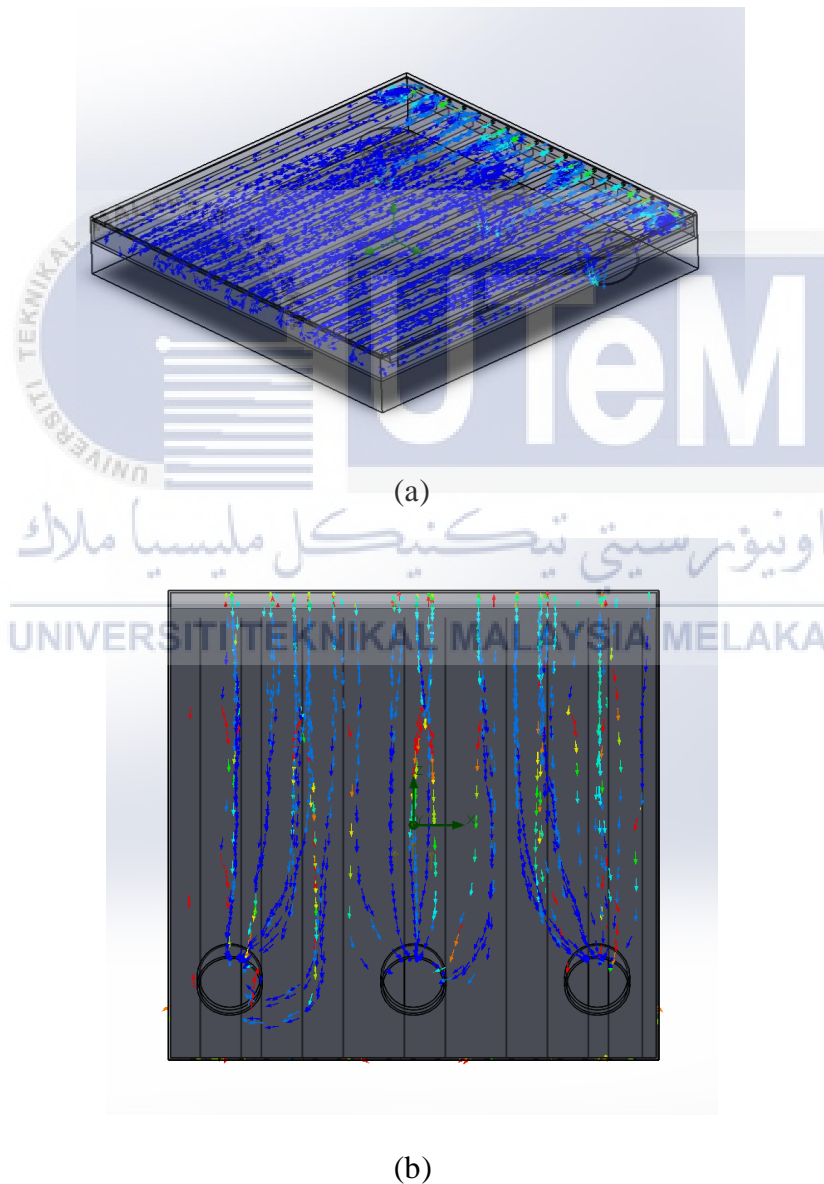


Figure. 4.2. Flow trajectories (a) top (b) bottom.

4.2 Result Validation

4.2.1 Study Model

The data taken as analysis parameters from the study model were taken using a digital anemometer and pyrometer.

Table. 4.1. Parameters of Study Model.

Parameters	Value
Irradiance (8/12/2021 @ 11.40 PM)	657 W/m ²
Initial Velocity	3.3 m/s
Ambient Temperature	30.7 °C / 303.85 K

The temperature on the absorber plate was recorded to validate the results for the CFD simulation. The location where the collection of temperature data will be taken from the absorber plate is shown in the model figure below:



Figure. 4.3. Marked Location for Recording Data.

The temperature will be recorded according to the marked location, left, middle and right, on the absorber. Several readings will be recorded at each location to have an average temperature.

The data recorded from the study model is recorded as the table below:

Table. 4.2. Temperatures Recorded in Marked Locations.

No of data	Temperature (K)		
	Left Absorber	Middle Absorber	Right Absorber
1	323.537	323.557	322.674
2	324.047	323.16	322.981
3	323.725	322.842	323.2
4	323.235	322.906	322.645
5	323.410	323.11	322.93
Average	323.590	323.115	322.89

The outlet temperature was recorded several times to find the average.

Table. 4.3. Average temperatures at the outlet.

No of data	Temperature (K)
	Study Model
1	314.55
2	315.05
3	314.7
4	313.84
5	314.372
Average	314.502

For both absorber temperature and outlet temperature, the average temperature was calculated.

4.2.2 CAD Model Based on Study Model

Table. 4.4. The temperature of Marked Location on CAD model based on study model.

No of data	Temperature (K)		
	Left Location Absorber	Middle Location Absorber	Right Location Absorber
1	324.85	324.45	320.55
2	325.95	322.75	323.75
3	326.05	325.25	325.35
4	325.95	325.75	325.65
5	325.67	324.33	323.01
Average	325.69	324.55	323.66

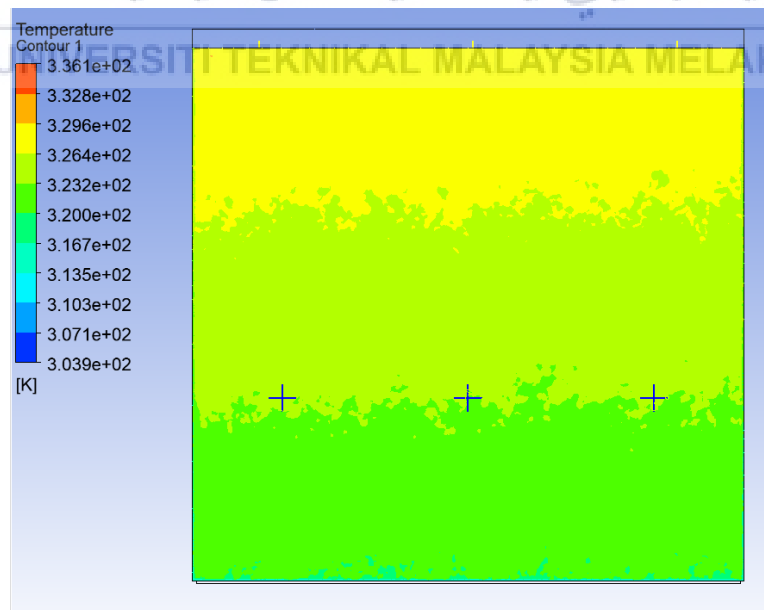


Figure. 4.4. Marked Location on CAD model based on study model.

Sama as data taken from the study model, the temperatures are taken from the CFD analysis are taken as average for each location.

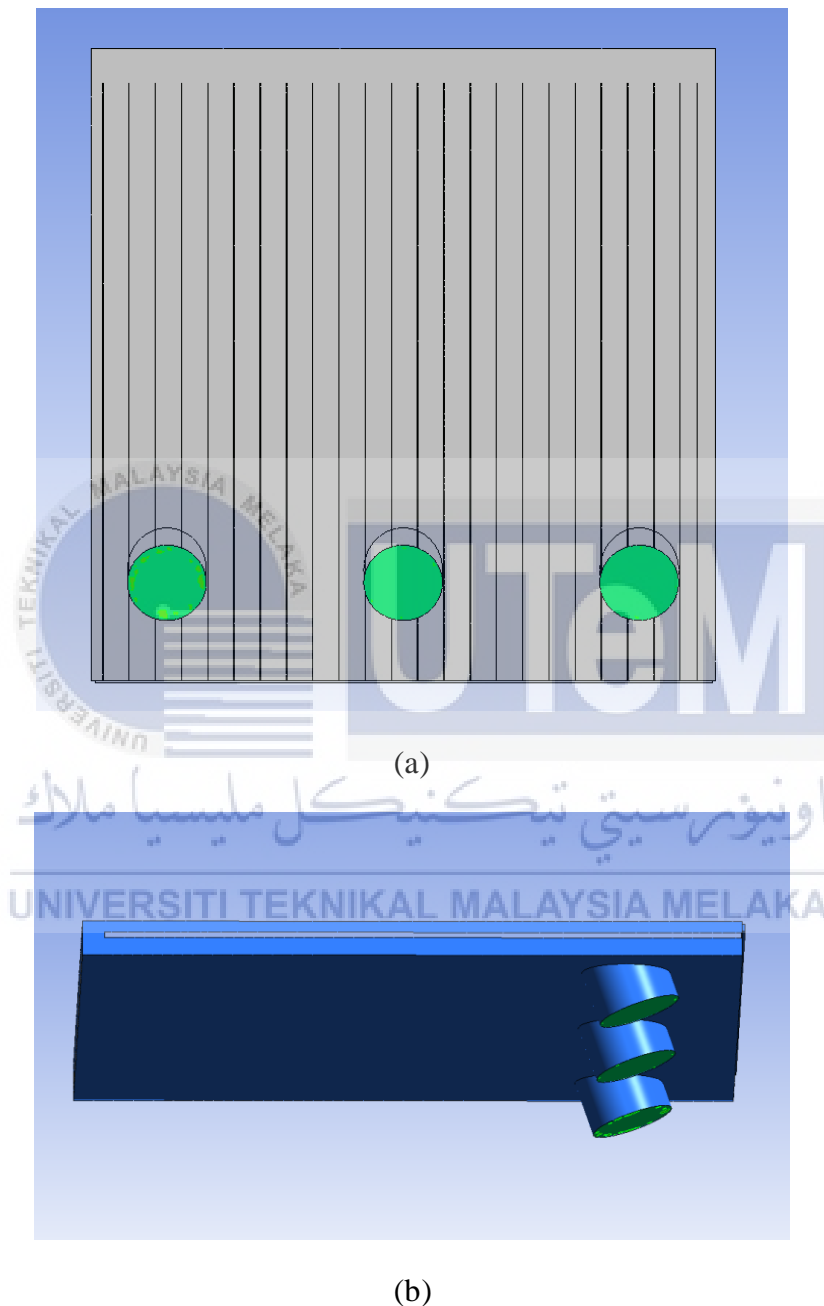


Figure. 4.5. Outlet Temperatures contour on CAD model based on study model. (a) Bottom
(b) Side.

4.3 Comparison between data taken from Study Model and CFD analysis

The temperature on the absorber was recorded several times and the average was calculated. The temperature of the absorber of the CAD model based on the study model using CFD was slightly higher than the study model.

Table. 4.5. Average Temperatures of Study Model and CFD.

Location	Average Temperature (K)		Percentage Difference (%)
	Study Model Data	CFD Analysis	
Absorber	323.2	324.63	0.44
Outlet	314.502	316.873	0.8

Figure 4.6 compares the study model to the CFD analysis using the study model in terms of temperature rise. Between the two, the temperature rise is roughly identical. As can be observed, the CFD values exceeded the data values generated by the research model. There is a discrepancy of approximately 2.3 K between the CFD and research model results. This demonstrates a high degree of agreement and acceptable forecast outcomes while performing CFD analysis. Due to the estimated heat loss for the insulation and flat-plate collector enclosure, the CFD values overpredict the outcomes of the study model. In physical environments, heat loss can never be zero, and it cannot be avoided.

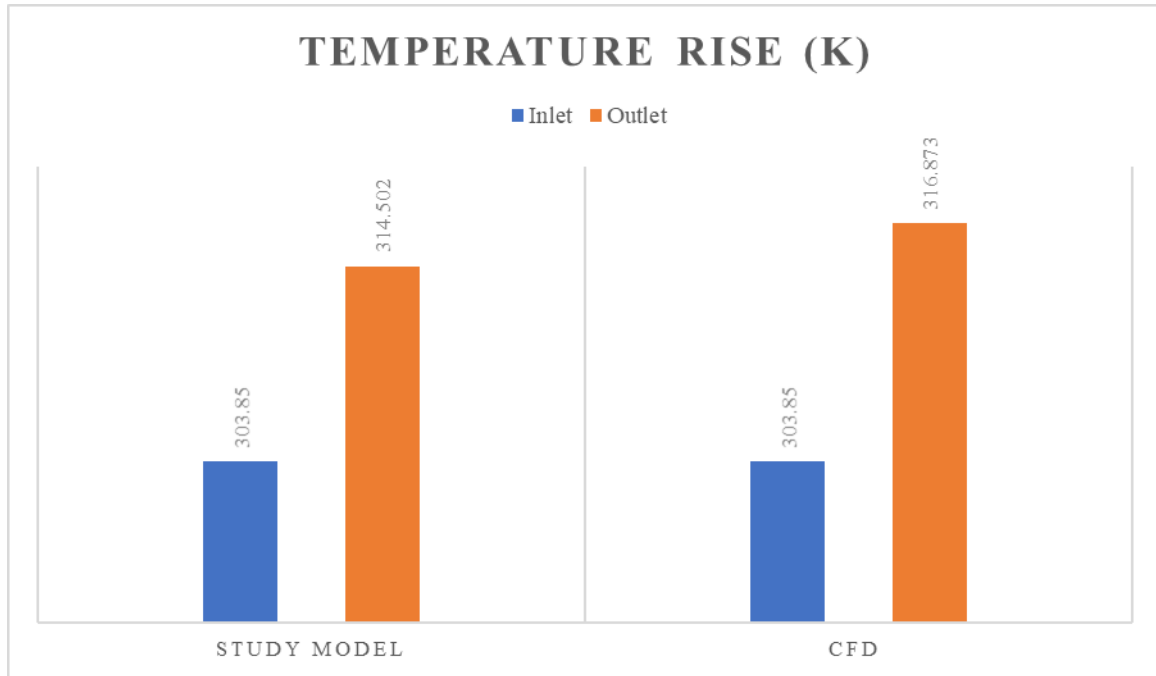
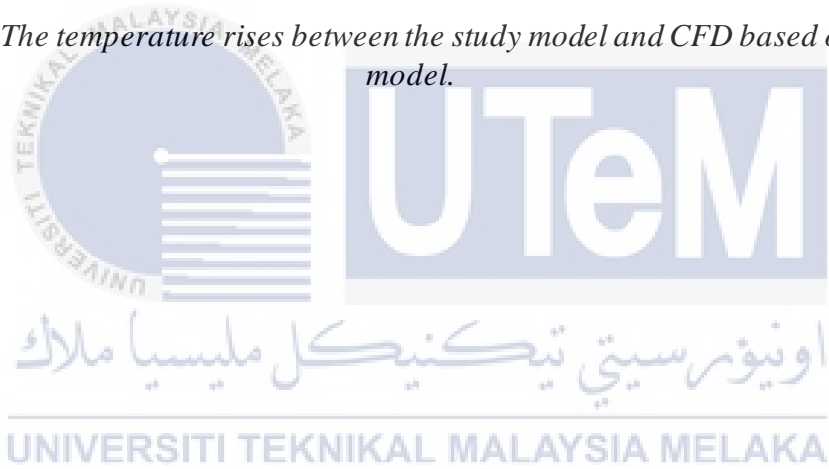
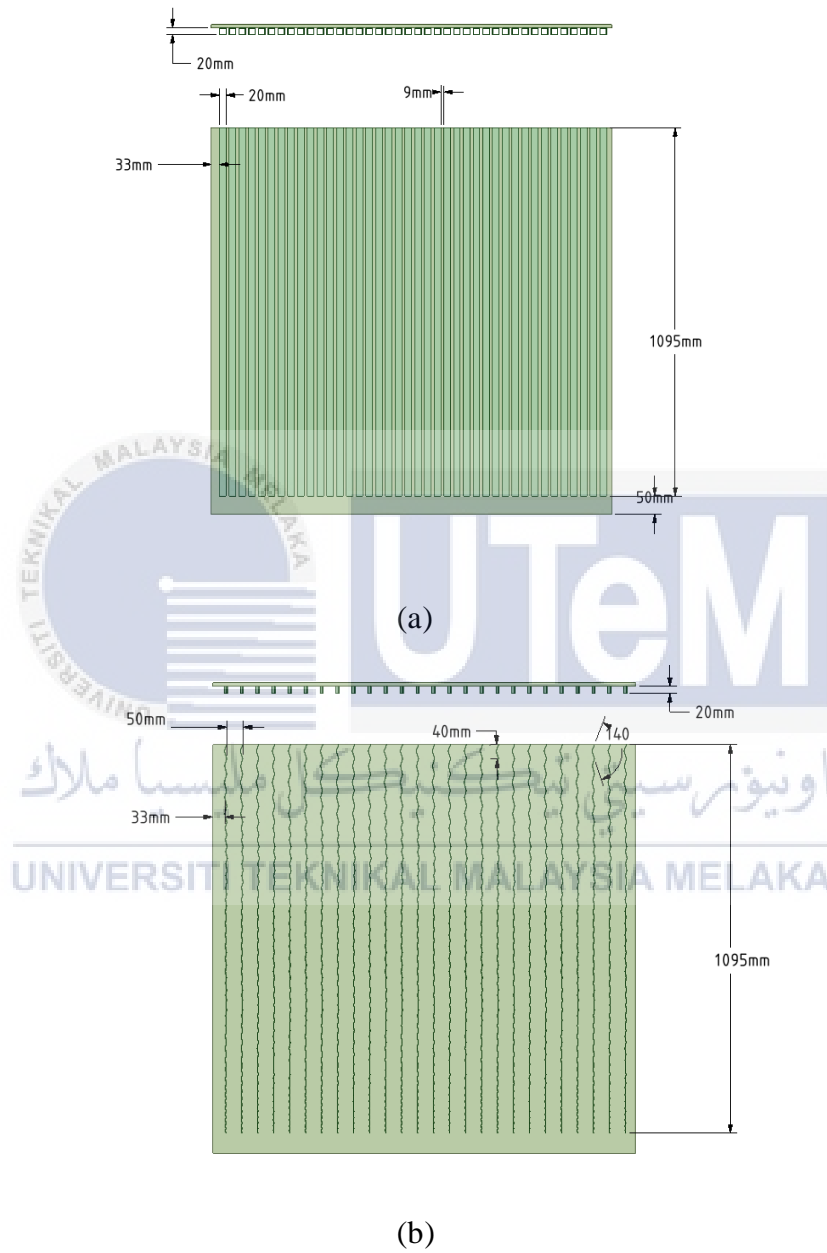
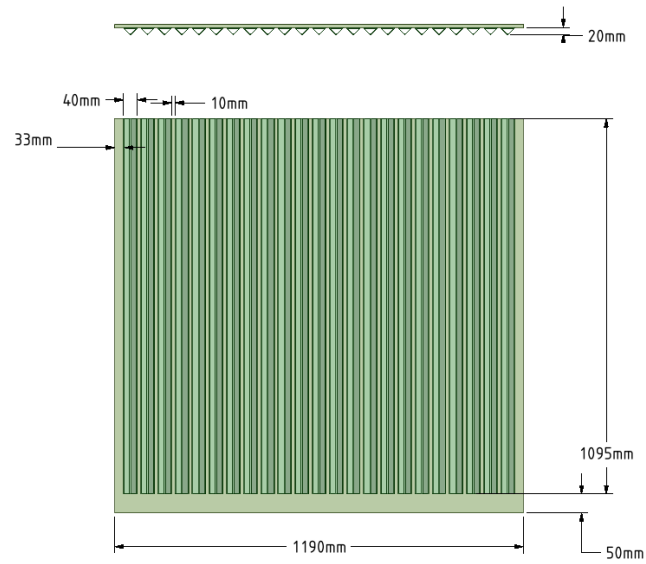


Figure. 4.6. The temperature rises between the study model and CFD based on the study model.

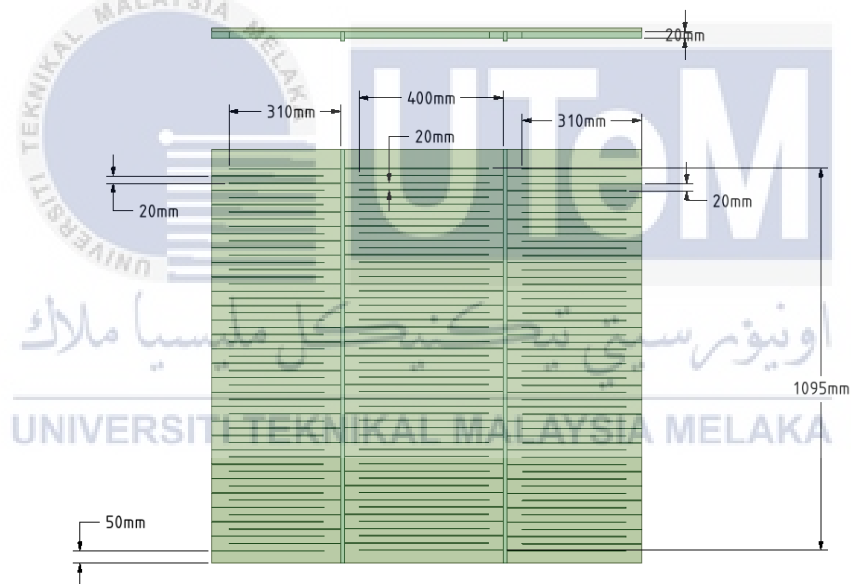


4.4 Fin Designs and the CFD Analysis





(c)



(d)

Figure. 4.7. Fins Design (a) Rectangular (b) Wavy (c) V-groove (d) Horizontal

4.4.1 Plain Fin Design (Study Model)

The results of temperatures around the fins for the study model were done by CFD.

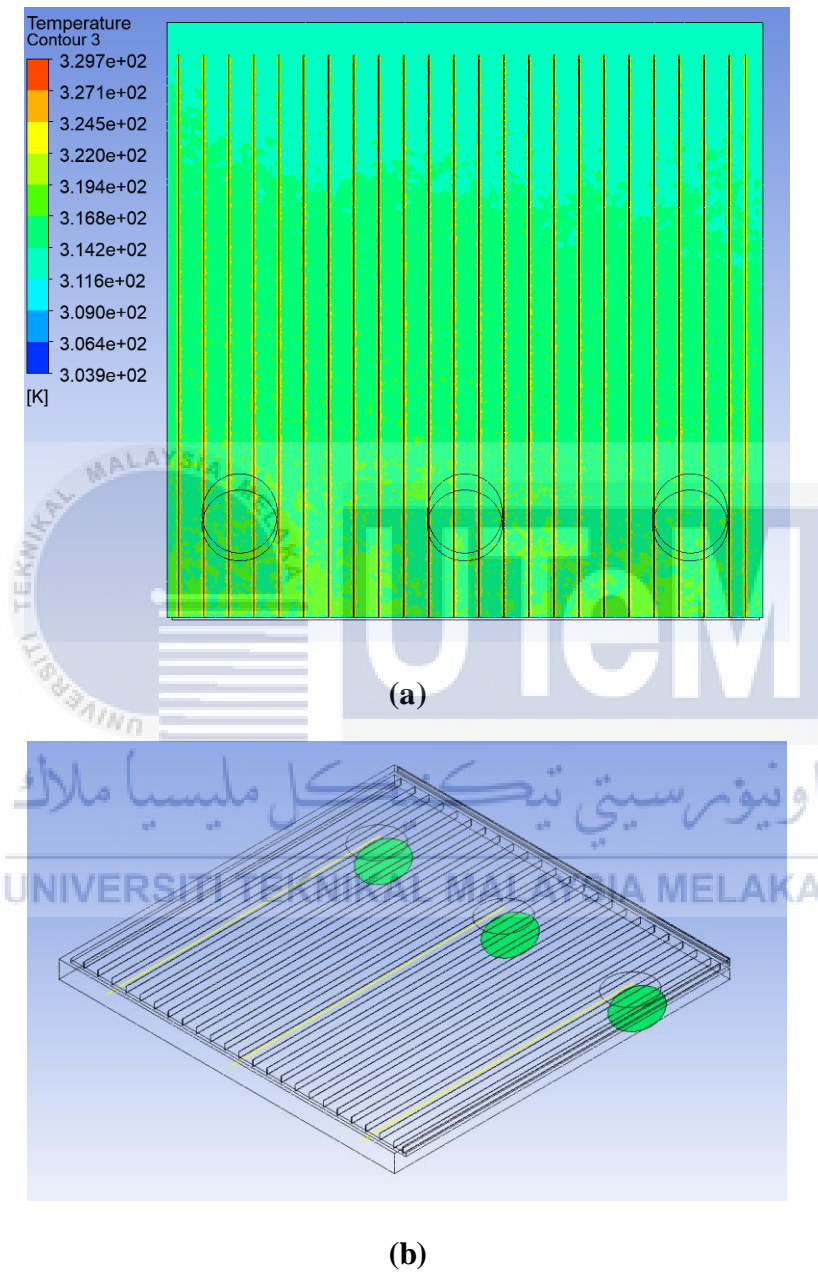
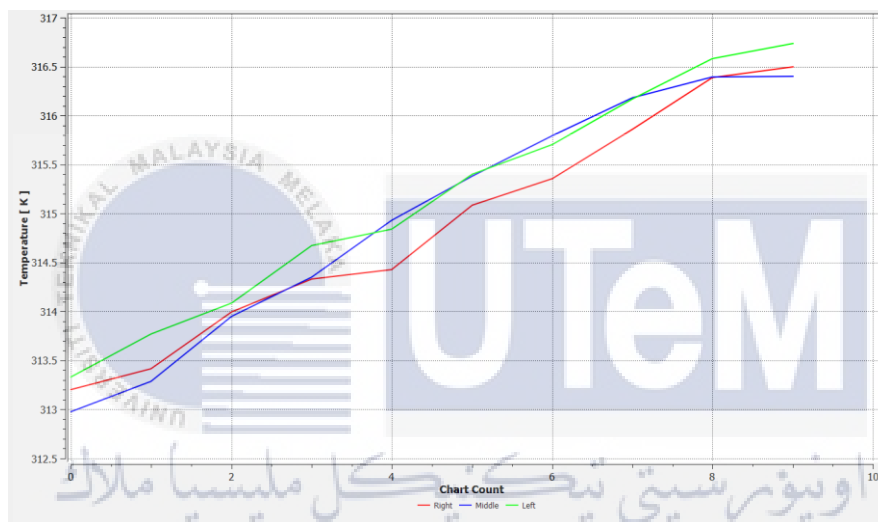


Figure. 4.8. (a) Temperature contour in fins region (b) Position where the results will be analyzed.

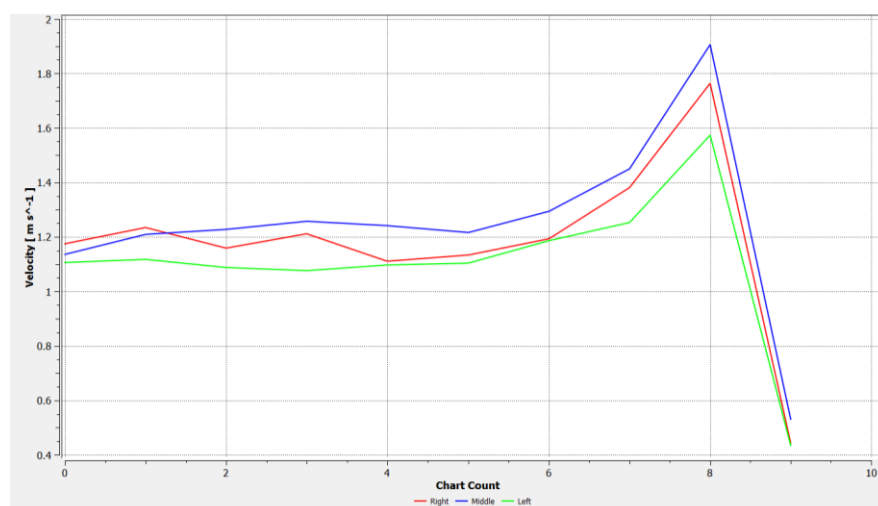
Several lines have been positioned to record the temperature rise between the fins.

Figure. 4.9 shows the results of the temperature rise and the velocity of CFD analysis for the study model. Figure. 4.9 (a) shows the temperature rise when the air flows through the fins. The graph shows the temperature is linearly increasing as the air flows through with a temperature maximum of approximately 316.75 K.

Figure. 4.9 (b) shows the velocity at the fins region steadily rising until, at a maximum of approximately 1.9 m/s and at one point, the velocity starts to drop. This is due to the airflow trajectories already entering the outlet region.



(a) UNIVERSITI TEKNIKAL MALAYSIA MELAKA



(b)

Figure. 4.9. Study Model (a) Temperature rise (b) Velocity.

4.4.2 Rectangular Fins

Figure. 4.10 and 4.11 show the design for rectangular fins and the CFD results overview in the rectangular fin region. Generally, the results show an improvement in the temperature of airflows when compared to the original study model.

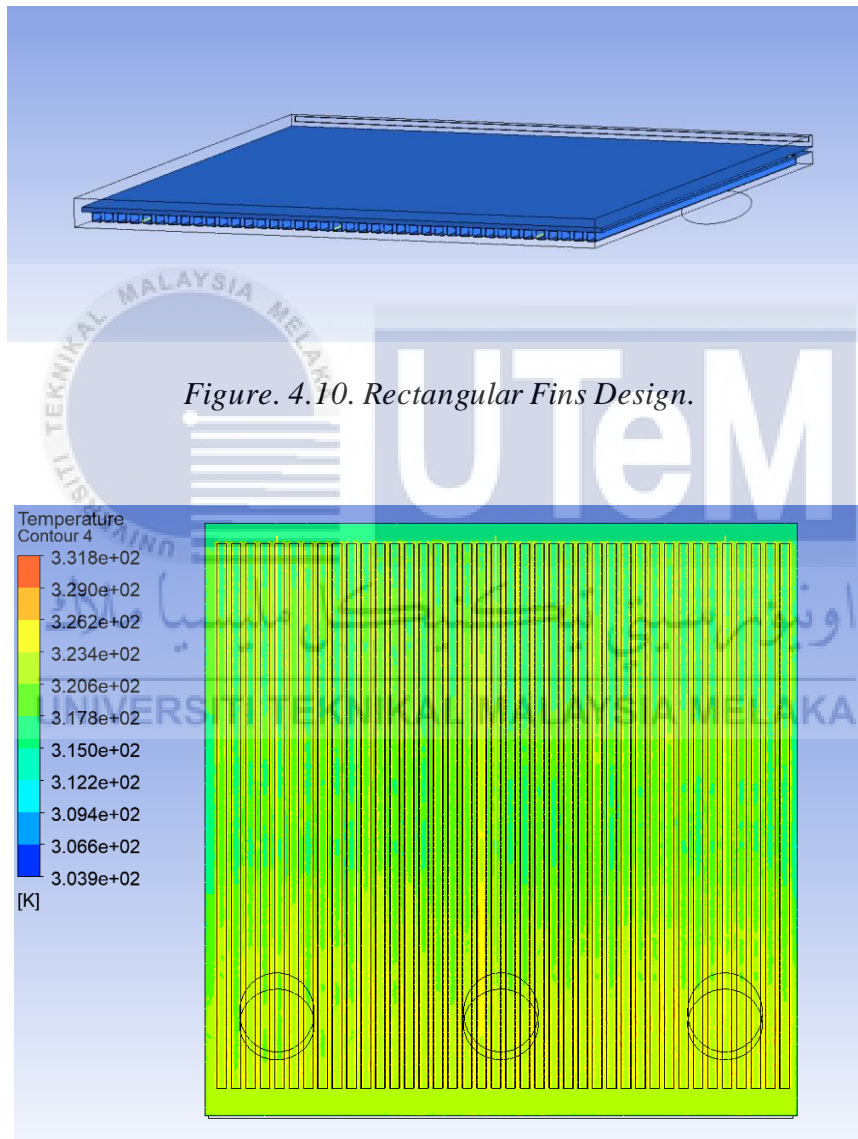
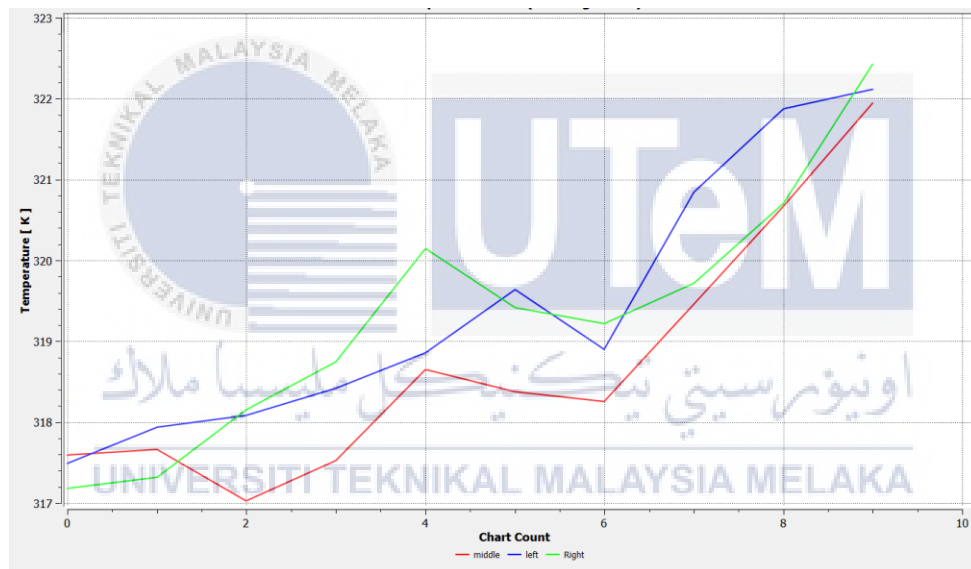


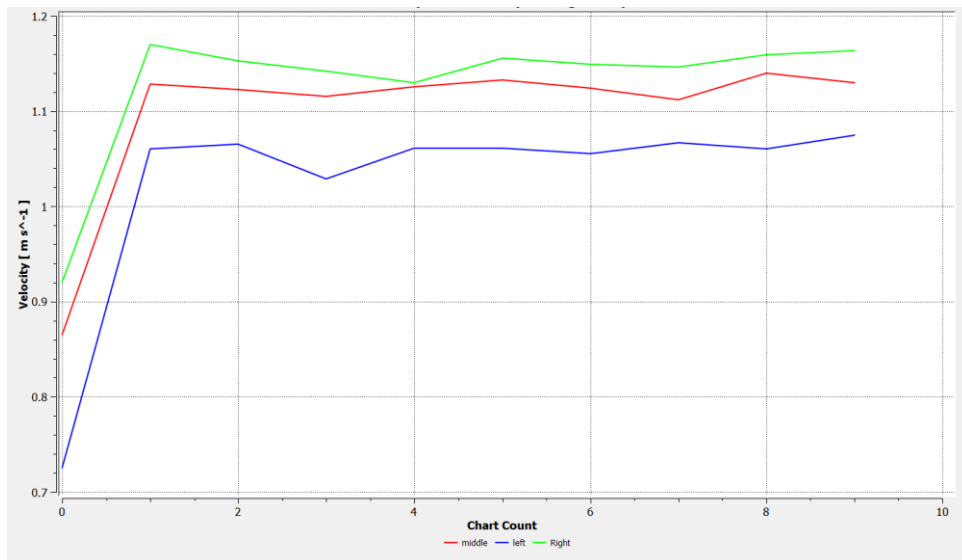
Figure. 4.11. Temperature contour in rectangular fins region.

Figure. 4.12 shows the results of the temperature rise and the velocity of CFD analysis for the rectangular fins design. Figure. 4.12 (a) shows the temperature rise when the air flows through the rectangular fins. The graph shows the overall temperature is higher than the study model while showing the same trend where the temperature is increasing as the air flows through the rectangular fins with a temperature maximum of approximately 322.4 K.

Figure. 4.12 (b) shows the velocity at the rectangular fins region steadily rising until the velocity flow is steady.



(a)



(b)

Figure. 4.12. Rectangular Fins (a) Temperature Rise (b) Velocity.

4.4.3 Wavy Fins

Figure. 4.13 and Figure. 4.14 show the design for wavy fins and the overview of temperature from CFD analysis in the wavy fin region. The figure shows the temperature in the wavy fin region. The overall temperature shows it is higher than the study model.

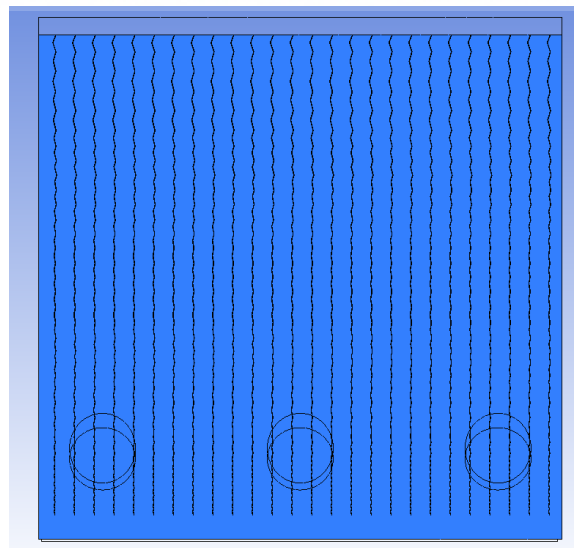


Figure. 4.13. Wavy Fins Design.

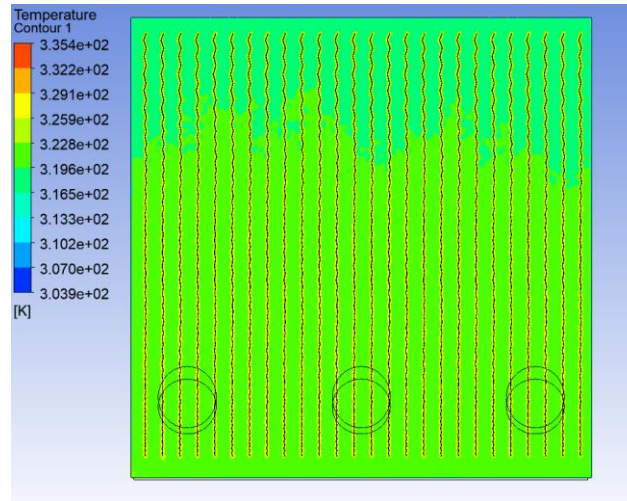
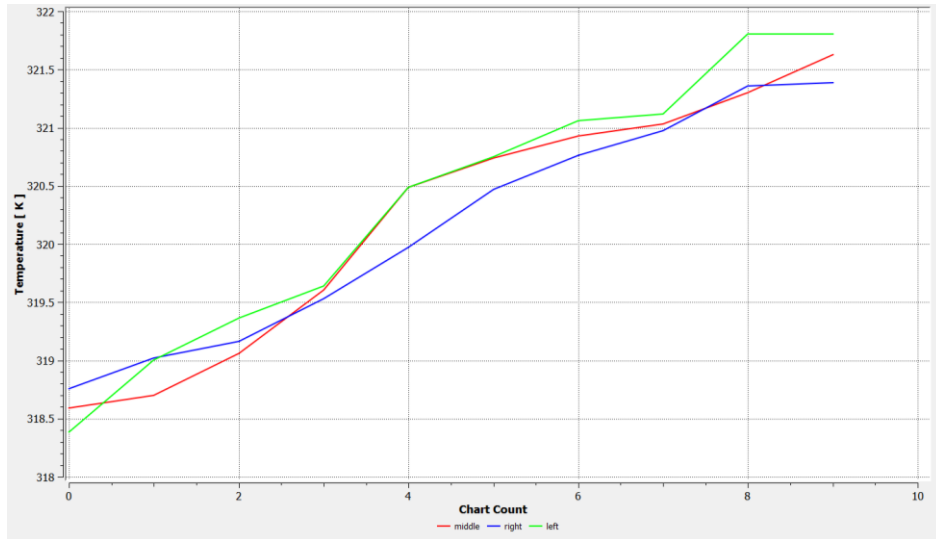


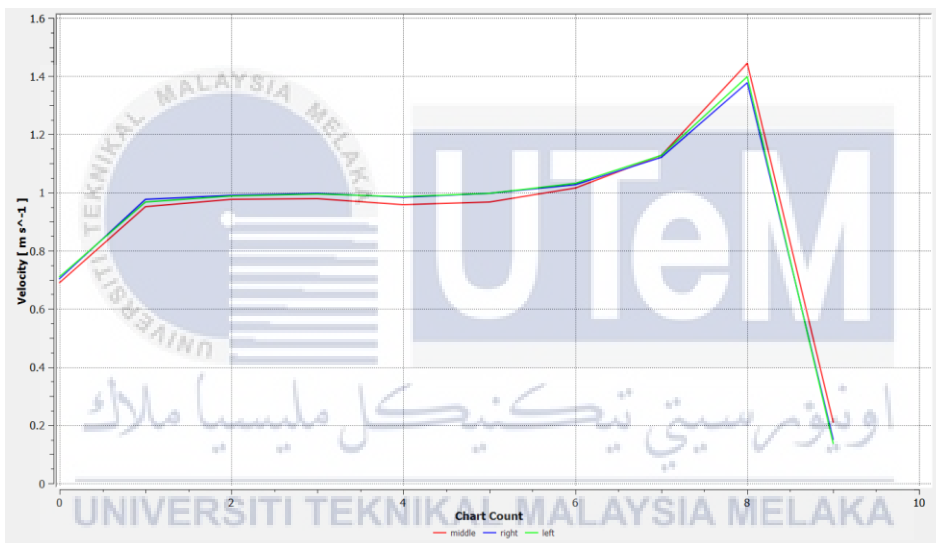
Figure. 4.14. Temperature Contour in Wavy Fins Region.

Figure. 4.15 (a) shows the results of the temperature rise of CFD analysis for the wavy fins design. The temperature rises as the air flows through the wavy fin region. The graph shows the overall temperature is higher than the study model while showing the same trend as the air flows through the wavy fins with a temperature maximum of approximately 321.8 K.

As for the velocity shown in Figure. 4.15 (b), the velocity shows a very similar trend as the study model.



(a)



(b)

Figure 4.15. Wavy Fins (a) Temperature rise (b) Velocity.

4.4.4 V- Groove Fins

Figures. 4.16 and 4.17 show the design for V-Groove Fins and the general overview of temperature in the v-groove fin region. The overall temperatures in the v-groove fin region are higher than the plain fin in the study model. This shows a similar result as rectangular fins where the temperature results have increased.

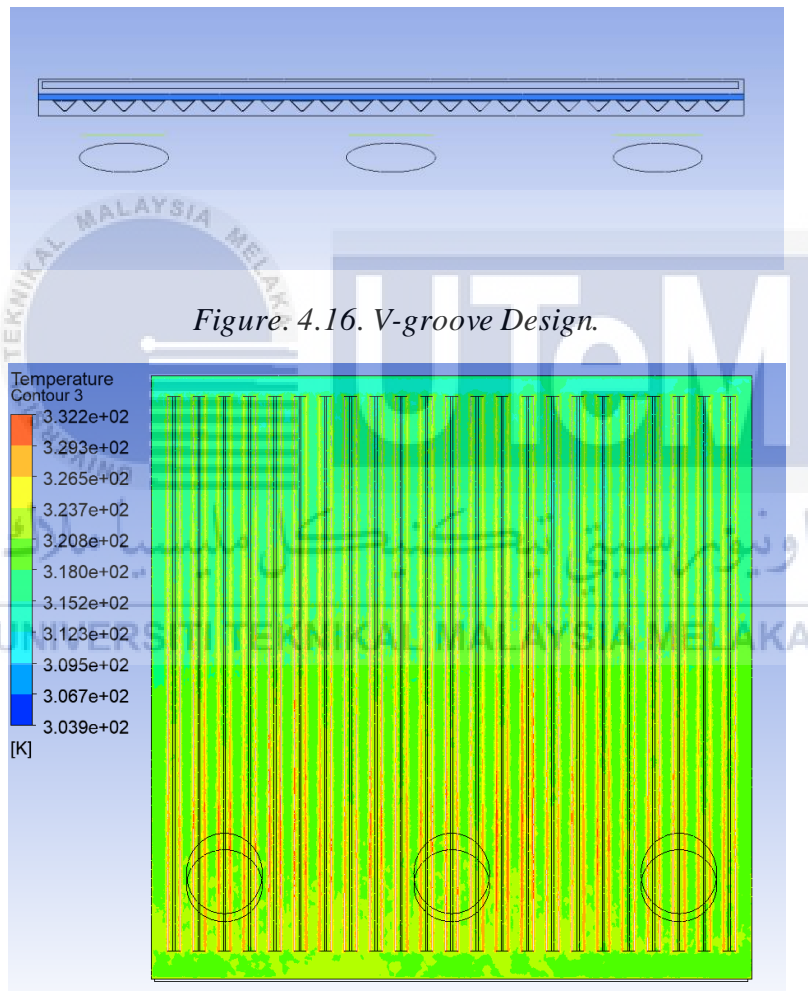
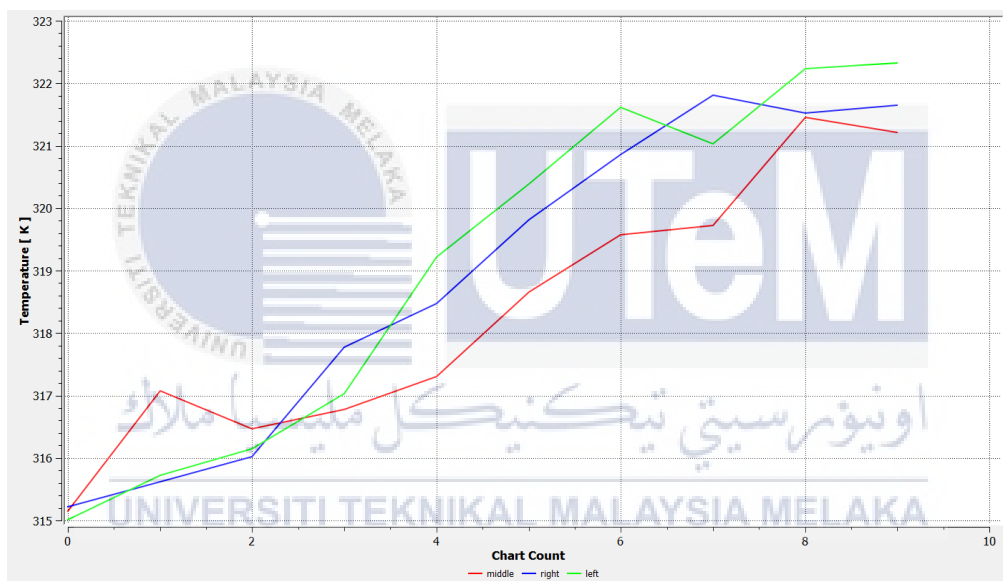
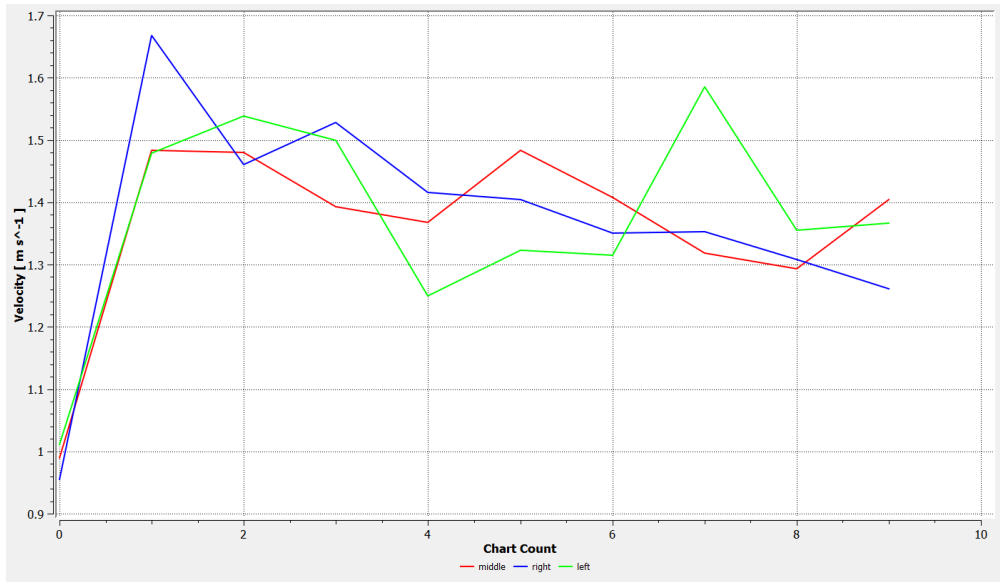


Figure. 4.18 shows the results of the temperature rise and the velocity of CFD analysis for the V-groove fins design. Figure. 4.18 (a) shows the temperature rise when the air flows through the v-groove fins. The graph shows the overall temperature is higher than the study model while showing the same trend where the temperature is increasing as the air flows through the v-groove fins with a temperature maximum of approximately 322.3 K.

Figure. 4.18 (b) shows the velocity at the v-groove fins region steadily rising until at a point where the velocity slightly drops upon approaching the outlet.



(a)



(b)

Figure 4.18. V-groove Fins (a) Temperature Rise (b) Velocity.



4.4.5 Horizontal Fins

Figures. 4.19 and 4.20 show the design for horizontal fins and the general overview of temperature in the horizontal fin region. The temperatures in the horizontal fin region are higher than the plain fin in the study model. This shows a similar result as rectangular fins and v-groove where the temperature results have increased.

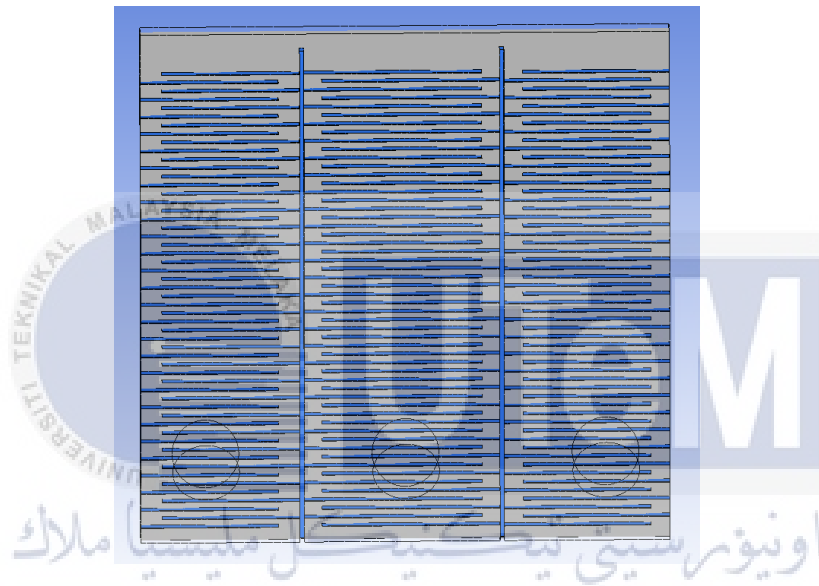


Figure. 4.19. Horizontal Fins Design.

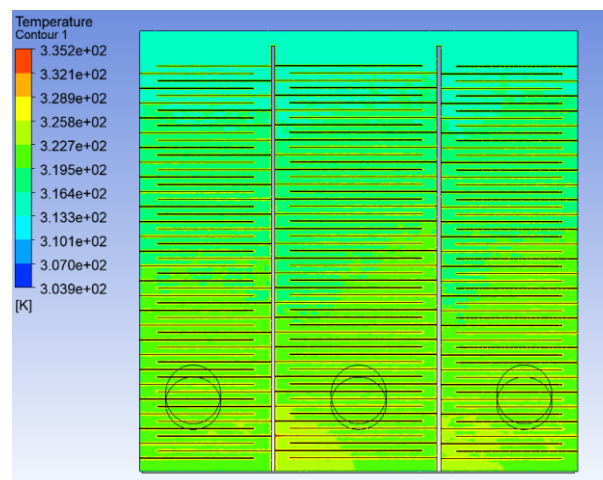
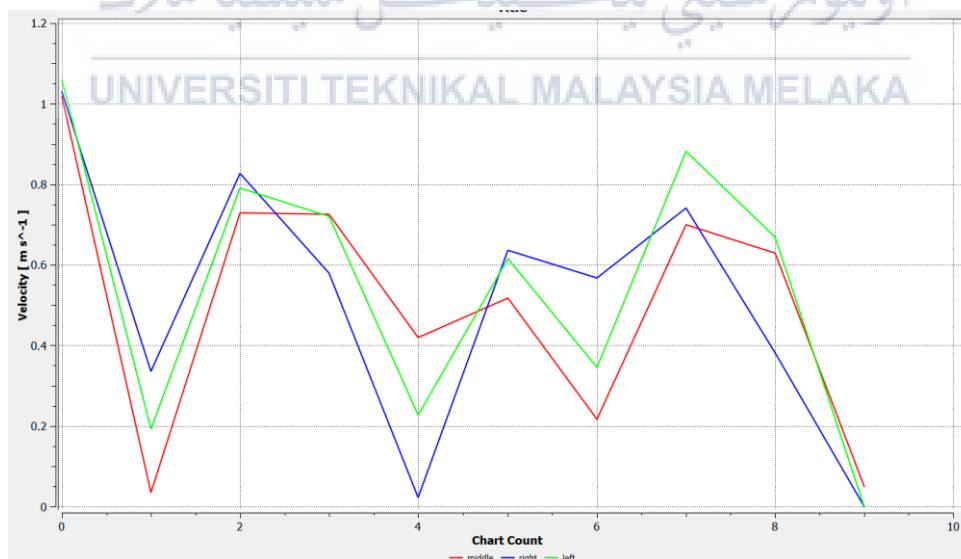


Figure. 4.20. Temperature Contour In horizontal fins region.

Figure. 4.21 (a) shows the temperature results in the horizontal fin region. Unlike the rectangular and v-groove fins, although the temperature increases, the graph for horizontal fins shows fluctuation in temperatures coherently with the velocity as shown in Figure. 4.21 (b). As the velocity increases, the temperature decreases.



(a)



(b)

Figure. 4.21. Horizontal Fins (a) Temperature rise (b) Velocity.

4.5 Results Discussion

4.5.1 The Effect of Fins on Temperature Rise

For each fin design, the average outlet temperature was taken as shown in Table. 4.6. It can be shown that, when compared to the study model, all the proposed designs have a larger surface area. Hence, it can be concluded that a large surface area has a higher average outlet temperature. Although, in the case of wavy and horizontal fins, how the airflow is affected by their geometry shapes instead of flowing linearly like the other designs, also affects the average outlet temperature.

Table. 4.6. Average Outlet Temperature of different Fins design configuration with their surface areas.

Design	Surface Area (mm ²)	Average Outlet Temperature (K)
Study Model	1703110	316.873
Rectangular Fins	6663680	320.807
Wavy Fins	2543215	321.675
V-groove Fins	4551471	320.537
Horizontal Fins	2423836	321.810

Figure. 4.22 shows the chart of temperature rise for each fin design and arrangement. The chart shows that rectangular, Wavy fins, v-groove, and horizontal has a higher temperature rise than the study model with a temperature difference of 5.4%, 5.6%, and 5.3% respectively while the horizontal fins are the highest with 5.7% when compared to the study model with only 4.2%.

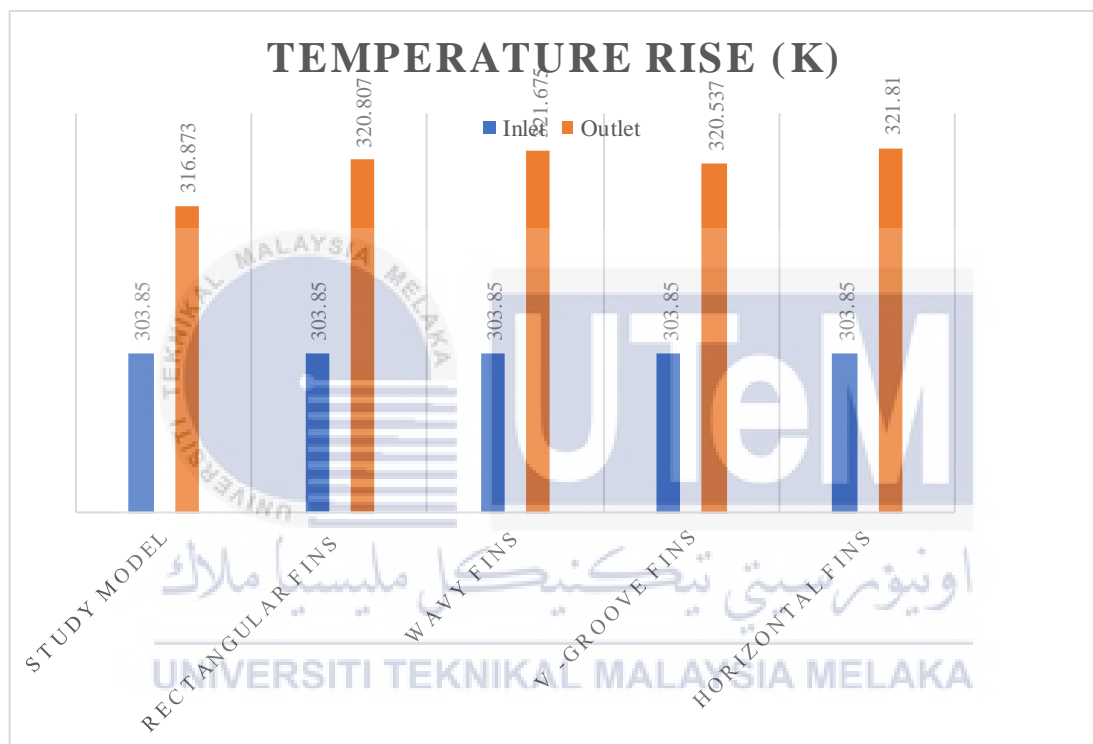
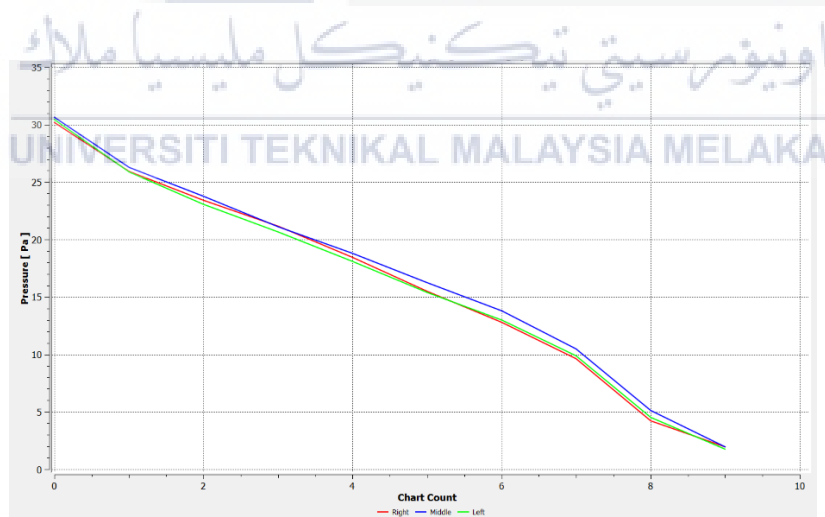


Figure. 4.22. Temperature Rise comparison between different types of fins configuration.

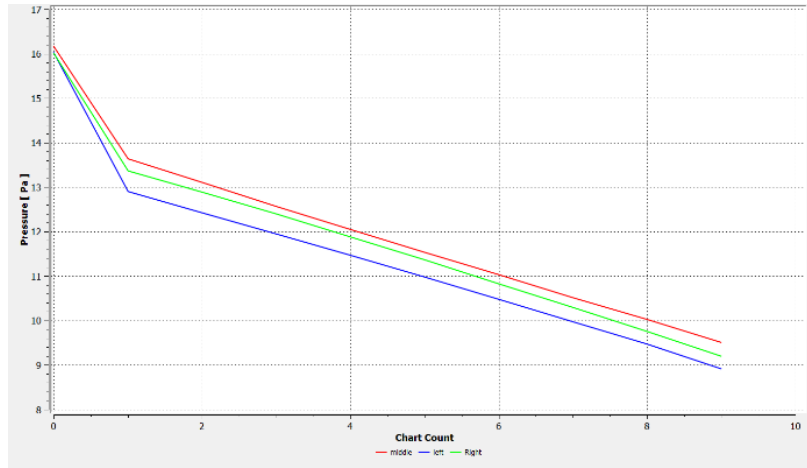
4.5.2 The Effect of Fins on Pressure in Solar Collectors

When the internal passageway of the collector channel, which in this example is the fins, is modified, the collector's thermal performance is improved, but the increased pressure drop across the collector is also increased. As the contact surface area grows, the pressure loss increases, necessitating greater pumping power for forced air convection. According to the pressure graph for each design shown in the picture. When air rushes through the fins and approaches the outlet, the pressure in the fins lowers. The pressure differential between all the designs is the greatest for horizontal fins and the least for wavy fins and the runners-up are the rectangular fins, v-groove fins, and lastly the study model.

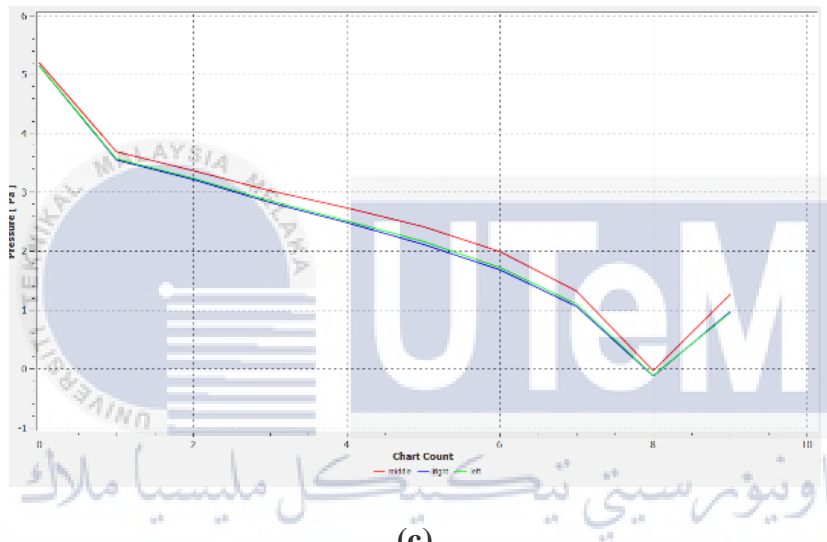
Although wavy fins have the least pressure difference, the overall pressure in the region is the lowest where it is important for airflow. Hence, the runners-up are likely to be considered as the best design, which is the rectangular fins and v-groove fins.



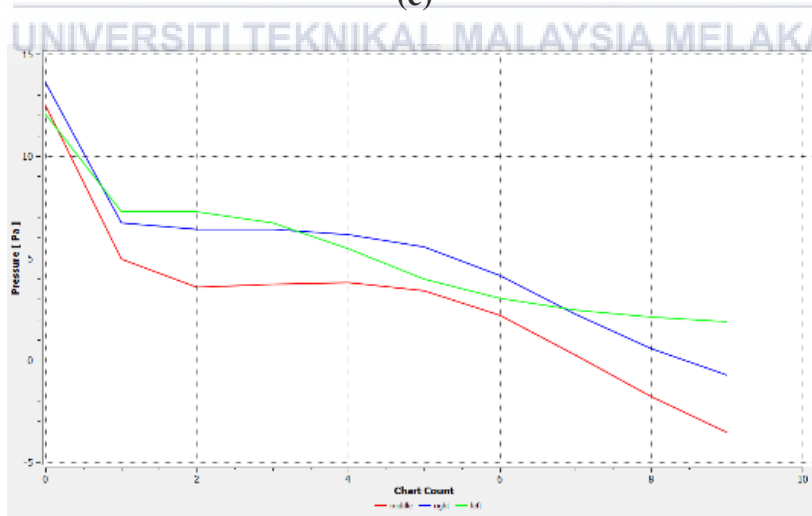
(a)



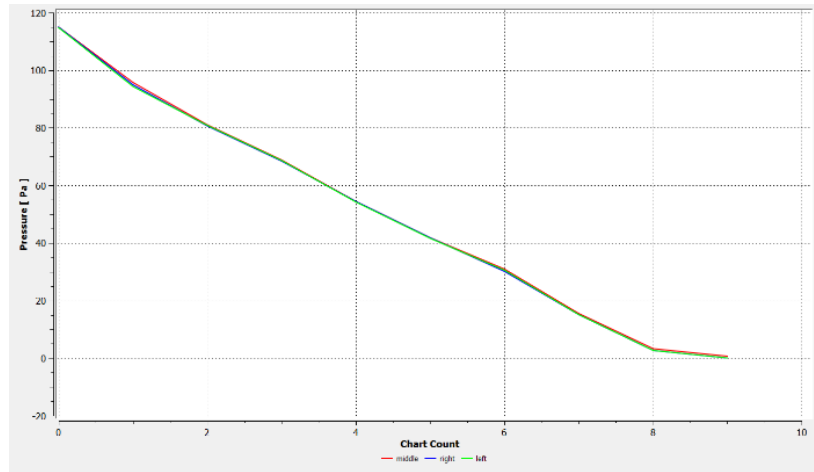
(b)



(c)



(d)



(e)

Figure. 4.23. Pressure on different fins design configurations.



Chapter 5

CONCLUSION

In a conclusion, the difference between experimental and CFD analysis of the absorber and the outlet temperature is 0.44% and 0.8% respectively. This shows a good agreement and acceptable results for CFD analysis. In the study, the fin configuration affects the performance of the solar collector. The arrangement and shape of the fins affect the temperature rise caused by heat absorption, air velocity, and pressure within the solar air collector. Apart from the research model, which consists of plain fins, the following configurations of fins were examined: rectangular, wavy, v-groove, and horizontal fins. All four of the newly recommended design fins configurations have a higher temperature than the study model. When compared to the temperature rises in the study model, horizontal fins had the largest temperature rises, while v-groove has the lowest temperature rises by a little margin over the other fin designs. However, the horizontal fins configuration has the biggest pressure drop of all the fin configurations, while the wavy fins configuration has the lowest pressure drop.

In summary, numerous aspects can influence the process of selecting the optimal design to improve the current study model as a recommendation for future work. Since the study model solar collector is being utilized to assist in the drying system application, one of the issues that should be considered is the cost-effectiveness of the upgrade and the power consumption. Although the horizontal fin has the fastest temperature rise, it is not worth choosing it over other designs to obtain the slightly higher temperature at the expense of more power used to pump the air to the outlet. Due to the small difference in temperature rise between the fin configurations, the best design to improve the current study model is the

rectangular fin, which has an acceptable pressure drop and is a cost-effective design to update due to its ease of implementation with the study model's current plain fins.



References

- AFSHARI, F., KHANLARI, A., SÖZEN, A., ŞİRİN, C., TUNCER, A. D., & GÜNGÖR, A. (2019). *CFD ANALYSIS ON FIN AND. Energy and Environmental Studies for the near future*, 84-93.
- Akpinar, E. K., & Koçyiğit, F. (2010). *Experimental investigation of thermal performance of solar air heater having different obstacles on absorber plates. International Communications in Heat and Mass Transfer*, 416-421.
- Biondi, P., Cicala, L., & Farina, G. (1988). *PERFORMANCE ANALYSIS OF SOLAR AIR HEATERS OF. solar energy*.
- Chokeman, Y., & Wongwises, S. (2005). *Effect of fin pattern on the air-side performance of herringbone. Heat Mass Transfer*.
- Close, D. J. (1963). *Solar Air Heaters For Low and Moderate Temperature Applications. Solar Energy*.
- Daliran, A., & Ajabshirchi, Y. (2018). *Theoretical and experimental research on effect. INFORMATION PROCESSING IN AGRICULTURE*.
- Elsafi, A., & Gandhidasan. (2015). *P. Performance of a Photovoltaic or Thermal Double - Pass Solar Air Heater with Different Fin Configurations. Clean Energy Techonology*, 28-33.
- Flynn, A., Akashige, T., & Theodore, L. (2019). *Kern's Process Heat Transfer*.
- Fudholi, A., & Sopian, K. (2018). *Review on Solar Collector for Agricultural Produce. International Journal of Power Electronics and Drive System*, 414-419.
- Fudholi, A., Sopian, K., Ruslan, M. H., & Othman, M. Y. (2013). *Performance and cost benefits analysis of double-pass solar collector. Energy Conversion and Management*.
- Gopi, R. (2014). *Experimental investigation of flat plate collector with cylindrical fins in a solar air heater*. 69-84.
- Ho, C.-D., Lin, C.-S., Chuang, Y.-C., & Chao, C.-C. (2013). *Performance improvement of wire mesh packed double-pass solar air heaters. Renewable Energy*.
- Ibtisam, A. (2018). *Enhancement the Performance of PV Panel by Using Fins as Heat Sink. Engineering Techonology*, 798-805.
- Incropera, F., & DeWitt, D. (1996). *Fundamentals of Heat and Mass Transfer*.
- Kannan, N., & Vakeesan, D. (2016). *Solar energy for future world: - A review. Renewable and Sustainable Energy Reviews*, 1092–1105.

- Kansara, R., Pathak, M., & Patel, V. K. (2021). *Performance assessment of flat-plate solar collector with internal fins and. International Journal of Thermal Sciences.*
- Karim, M. A., & Hawlader, M. (2005). *Performance evaluation of a v-groove solar air collector. Applied Thermal Engineering.*
- Karsli, S. (2007). *Performance analysis of new-design solar air collectors for drying applications. Renewable Energy, 1645-1660.*
- Khatib, T., Mohamed, A., Mahmoud, M., & Sopian, K. (2015). *Optimization of the Tilt Angle of Solar Panels for Malaysia. Energy Sources, 606-613.*
- Kim, J., & Nam, Y. (2019). *Study on the Cooling Effect of Attached Fins on PV. Energies , 758.*
- Koundinya, S., & Krishnan, A. (2014). *Computational Study of Cooling of PV solar panel using finned heat pipe. 216-223.*
- Krauter, S., & Preiss, A. (2009). *Comparison of Module Temperature Measurement Methods.*
- Kumar, R., & Chand, P. (2017). *Performance Enhancement of Solar Air Heater using Herringbone. Energy, 271-279.*
- Kumar, S., & Saini, R. (2009). *CFD based performance analysis of a solar air heater duct provided with artificial roughness. Renewable energy, 1285-1291.*
- Lingayat, A., Chandramohan, V., & Raju, V. (2018). *Numerical analysis on solar air collector provided with artificial square shaped roughness for indirect type solar dryer. Journal of Cleaner Production , 353-367.*
- Mohamad, A. A. (1997). *HIGH EFFICIENCY SOLAR AIR HEATER. Solar Energy .*
- Momin, A.-M. E., Saini, J., & Solanki, S. (2002). *Heat transfer and friction in solar air heater duct with V-shaped rib roughness on absorber plate. International Journal of Heat and Mass Transfer.*
- Naphon, P. (2005). *On the performance and entropy generation of the. Renewable Energy , 1345-1357.*
- Priyam, A., & Chand, P. (2016). *Thermal and thermohydraulic performance of wavy finned absorber solar air heater. Solar Energy, 250-259.*
- Rai, S., Chand, P., & Sharma, S. P. (2017). *An analytical investigations on thermal and thermohydraulic performance of offset finned absorber solar air heater. Solar Energy , 25-40.*
- Roache, P. (1998). *Perspective: a method for uniform reporting of grid refinement studies . Fluids Engineering, 405-413.*

- Singh Yadav, A., & Kumar Thapak, M. (2014). Artificially roughened solar air heater: Experimental investigations. *Renewable and Sustainable Energy Reviews* , 370-411.
- Singh, S. (2020). Thermohydraulic performance of double pass solar thermal collector with inline, staggered and hybrid fin configurations. *Journal of energy storage* .
- Singh, S., & Dhiman, P. (2015). Thermal and Thermohydraulic Efficiency of Recyclic-Type Double-Pass Solar Air Heaters With Fins and Baffles. *Heat Transfer Engineering*, 1302-1317.
- Singh, S., & Dhiman, P. (2016). Thermal performance analysis of a rectangular longitudinal. *Solar Energy Engineering* .
- Singh, S., Chander, S., & Saini, J. S. (2015). Thermo-hydraulic performance due to relative roughness pitch in V-down rib with gap in solar air heater duct—Comparison with similar rib roughness geometries. . *Renewable and Sustainable Energy Reviews*, 1159-1166.
- Solangi, K. H., Islam, M. R., Saidur, R., Rahim , N. A., & Fayaz, H. (2011). A review of global solar energy solar policy. *Renewable and Sustainable Energy Reviews* , 2149-2163.
- Taieb, N., Mohamed, B., & Driss, N. (2016). Effect of the Fins Length for the Passive Cooling of the Photovoltaic Panels. 28-33.
- Tian, Y., & Zhao , C. Y. (2013). A review of solar collectors and thermal energy storage in solar thermal applications. *Applied Energy*, 538–553.
- Vyas, S., & Punjabi, D. S. (2014). THERMAL PERFORMANCE TESTING OF A FLAT PLATE SOLAR AIR HEATER USING OPTICAL MEASUREMENT TECHNIQUE. *International Journal of Recent advances in Mechanical Engineering*, 69-84.
- Xiangtao, G., Fuqiang, W., Haiyan, W., Jianyu, T., Qingzhi, L., & Huaizhi, H. (2017). Heat transfer enhancement analysis of tube receiver for parabolic trough. *Solar Energy*.
- Yadav, A. S., & Bhagoria, J. (2013). Heat transfer and fluid flow analysis of solar air heater: A review of CFD approach. *Renewable and Sustainable Energy Reviews*, 60-79.